IDENTIFICATION AND FUNCTIONAL CHARACTERIZATION OF P113 AS A NOVEL BLOOD-STAGE VACCINE TARGET AGAINST SEVERE PLASMODIUM FALCIPARUM MALARIA

By

YIYU ZHENG

BS, BUCKNELL UNIVERSITY, 2024

Thesis

Submitted in partial fulfillment of the requirements for the Degree of Master of Science in the Graduate Program of Biotechnology at Brown University

PROVIDENCE, RHODE ISLAND

MAY 2026

This thesis by Yiyu Zheng is accepted in its present form by the Graduate Program in Biotechnology as satisfying the thesis requirements for the degree of Master of Science

Date_____ Signature: _____

Dr. Jonathan D. Kurtis, Advisor

Date_____ Signature: _____

Dr. Hannah Wu, Reader

Date_____ Signature: _____

Dr. Tanbir Najrana, Reader

Approved by the Graduate Council

Date_____ Signature: _____

Dr. David P. Lindstrom, Dean of the Graduate School

Acknowledgements

I would like to begin by expressing my deepest gratitude to my thesis advisor, Dr. Jonathan D. Kurtis, for welcoming me into the lab and for his generosity, patience, and unwavering support throughout my time at Brown. His mentorship has been truly invaluable, and I am incredibly thankful for the opportunity to learn and grow under his guidance.

I am sincerely grateful to my project advisor, Dr. Brajesh K. Singh, whose dedication and depth of knowledge in research and beyond have been truly inspiring for me. His passion, perspective, and commitment serve as a role model for me, and I feel fortunate to have learned from him.

I would also like to extend my heartfelt thanks to Dr. Hannah Wu for her kindness, encouragement, and guidance both inside and beyond the lab. I am deeply appreciative of Lilianna Hammons and Sunthorn Pond-Tor for their patience and generosity in teaching me the foundational techniques and skills for the work that I did. I am grateful to Kanika Men, Ben Moore, and Teja Prakash for their support and willingness to lend a helping hand at every stage.

Thank you to the Brown SPS CMX team for their mentorship, encouragement, and the sense of community they provided. The experiences and memories we shared have made my journey at Brown more meaningful!

A very special thank you to my best cat/roommate, Fauna, for her companionship and emotional support. Lastly, I am profoundly grateful to my parents for their unconditional love, patience, and belief in me. Your support has been my foundation, and I would not be here without you!

Table of Contents

Table of Figures

Table of Tables

Abstract of "Identification and Functional Characterization of P113 as a Novel Blood-Stage Vaccine Target Against Severe Plasmodium falciparum Malaria", by Yiyu Zheng, ScM, Brown University, May 2026

Malaria is a leading cause of child mortality worldwide and a significant burden on global health. The severe malaria (SM) subtype is particularly consequential, carrying a case fatality rate of 20%. Although pre-erythrocytic vaccines such as RTS,S/AS01 and R21/Matrix-M have been approved for malaria prevention, they are limited in targeting SM cases, as their efficacy diminishes over time due to parasite resistance, and neither targets blood-stage parasites directly, which are especially responsible for SM pathology. Previous studies have shown that naturally acquired immunity to SM develops rapidly, usually after only one or two episodes. Since this immunity is mediated primarily by antibodies, this study aimed to identify the specific parasite antigens targeted by these protective responses.

In this thesis, we performed whole-proteome differential screening (WPDS) using post-SM plasma from our Kenyan cohort and a *Plasmodium falciparum* 3D7 cDNA library displayed in T7 phage, leading to the identification of 46 parasite proteins uniquely recognized by antibodies from children with severe malaria. Among these candidates, we prioritized PfP113 (P113; PF3D7_1420700) based on its enrichment, biochemical features, and biological relevance. P113 is a 112.6-kDa GPI-anchored merozoite surface protein which anchors the PfRh5 invasion complex to the merozoite surface and displays limited sequence variation across field isolates, making it an attractive vaccine candidate. PfGARP is a previously validated vaccine target from the Kurtis Laboratory, was independently recovered in the screen (34.4% of fourth-round clones) and was utilized as an internal positive control.

Recombinant P113 was expressed in Expi293F cells, purified by nickel-column immobilized metal affinity chromatography, and validated by LC-MS/MS mass spectrometry.

Mice (BALB/c) immunized with recombinant P113 formulated with TiterMax Gold adjuvant developed anti-P113 antibodies. However, only ~20% of immunized mice (out of 45 mice, with initial cohort of 5 showing 1 responder) produced sera with growth-inhibitory activity against P. falciparum 3D7 parasites in vitro, as measured by growth inhibition assay.

Comparison of inhibitory and non-inhibitory sera indicated that both groups had comparable antibody titers and both recognized native P113 in parasite lysates by Western blot. This demonstrates that the growth-inhibitory phenotype is not determined by antibody quantity or overall antigen recognition. Epitope mapping revealed that inhibitory and non-inhibitory sera shared broadly similar binding profiles, yet the inhibitory sera uniquely recognized a shifted epitope, HLQGSEQSIEASESS, which suggests that antibodies targeting this specific region may be responsible for functional parasite growth inhibition.

Collectively, these findings advance P113 from a bioinformatically identified candidate to a functionally validated blood-stage vaccine antigen. This study also provides the first evidence that immunization-induced anti-P113 antibodies can inhibit *P. falciparum* growth. The identification of a candidate inhibitory epitope establishes a foundation for focused peptide–conjugate immunization strategies aimed at improving the responder rate. This work contributes to the expanding repertoire of blood-stage antigens targeting severe *P. falciparum* malaria and supports the development of P113 as a component of a multi-antigen vaccine strategy.

Chapter 1: Introduction

1.1 Global Burden of Malaria

Malaria remains one of the most deadly infectious diseases threatening global public health. The disease is transmitted to humans through the bite of infected female *Anopheles* mosquitoes and caused by protozoan parasites of the genus *Plasmodium*. There are five species that are known to infect humans: *P. falciparum, P. vivax, P. ovale, P. malariae,* and *P. knowlesi*. Severe and fatal cases are almost exclusively caused by *P. falciparum.*[1]

According to the latest World Malaria Report by the World Health Organization (WHO) from 2024, there were 282 million cases of malaria and 610,000 deaths worldwide.[2] This burden is heavily concentrated in sub-Saharan Africa, where approximately 95% of malaria cases worldwide are located (Figure 1). Children under five show a disproportionate mortality rate, accounting for about 80% of all malaria-related fatalities in Africa.[2] Other vulnerable populations include pregnant women, as malaria parasites preferentially sequester in the placenta. This leads to maternal anemia and adverse pregnancy outcomes, including stillbirth, preterm delivery, and low birth weight.[3]

The latest Global Burden of Disease Study 2023 (GBD 2023) further identifies malaria as the leading global health burden of any single-agent pathogenic disease, measured in disability-adjusted life years (DALYs).[4] Compared to HIV/AIDS (45 million) and tuberculosis (44 million), malaria has an estimated 52 million DALYs, along with heavy economic consequences.[4] A study from Harvard's Center for International Development explicitly demonstrated that, after controlling for socioeconomic and geographic factors, countries with the highest malaria burden experienced 1.3% lower annual growth in GDP per capita between 1965 and 1990 compared to malaria-free countries.[5] This growth gap implies that a country facing the

maximum malaria burden would attain a GDP per capita only 27% of that of an otherwise identical malaria-free country over the course of a century.[5]

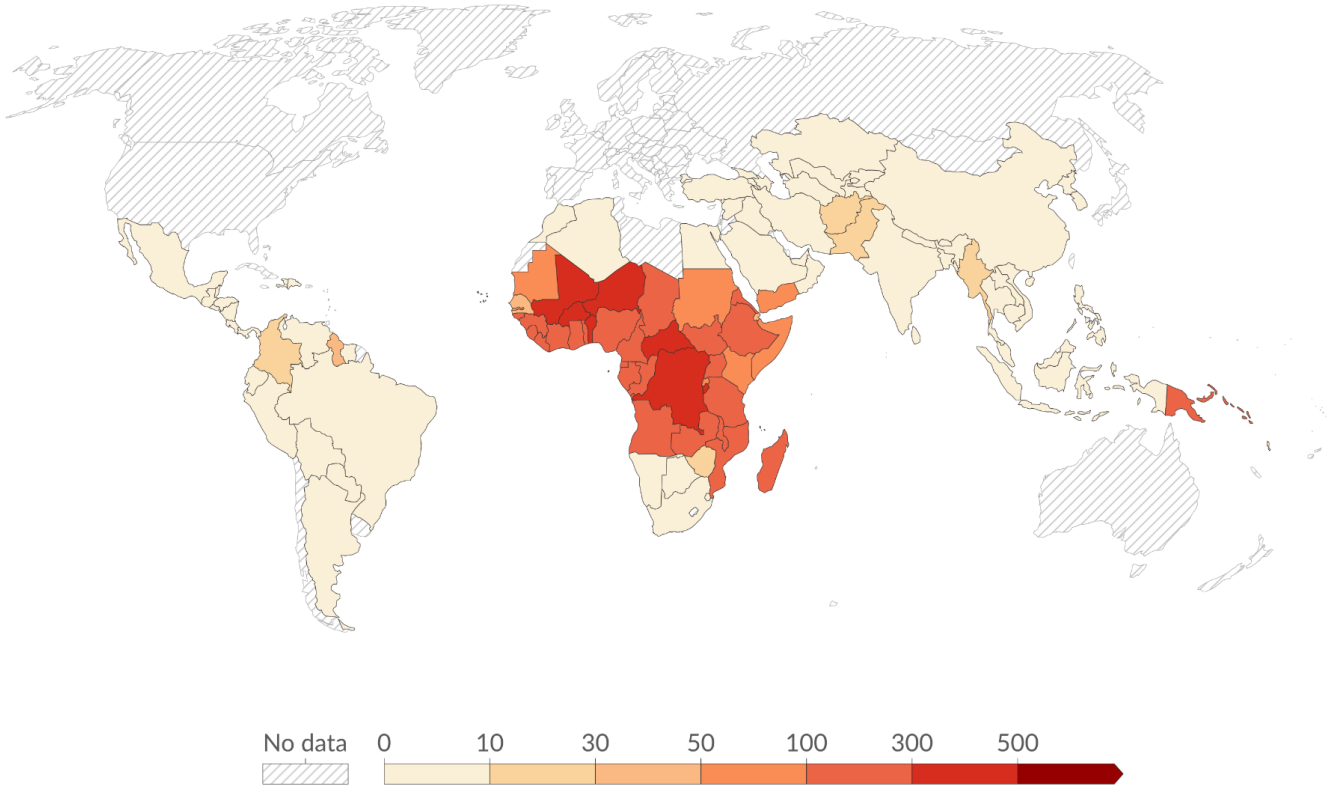

Figure 1. Global distribution of malaria incidence, 2024. New cases of malaria per 1,000 people at risk by country, based on data from the WHO Global Health Observatory via the World Bank. The burden is overwhelmingly concentrated in sub-Saharan Africa, with the highest incidence rates (>300 per 1,000) observed in West and Central African nations. Regions of Southeast Asia and Oceania also bear significant transmission. Reproduced from Our World in Data [37]; licensed under CC BY 4.0.

1.2 Plasmodium falciparum Life Cycle and Pathogenesis

The life cycle of *P. falciparum* involves both the mosquito vector and the human host. Infection begins when an infected female *Anopheles* mosquito inoculates sporozoites into humans during a blood meal. These sporozoites travel rapidly to the liver, where they invade

hepatocytes. Over approximately two weeks, they will undergo asexual replication and produce tens of thousands of merozoites per infected hepatocyte. This liver or pre-erythrocytic stage is clinically silent.[6]

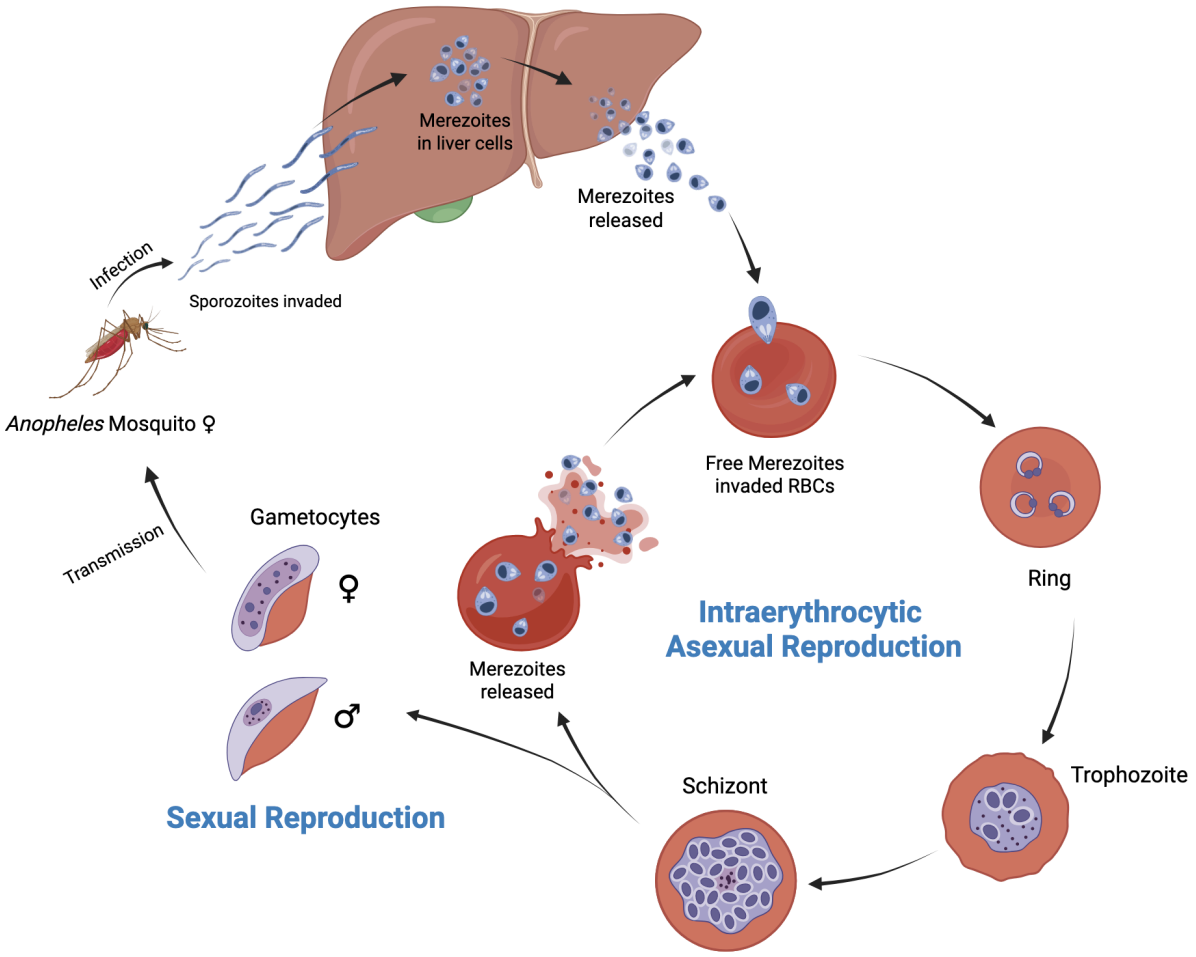

Figure 2. Life cycle of *P. falciparum*. Figure created with BioRender.com; adapted from Microbe Notes.[30]

When the hepatocytes rupture, merozoites are released into the bloodstream initiating the erythrocytic cycle. This stage shows all of the clinical manifestations of malaria. Through ligand-receptor interactions, merozoites invade red blood cells (RBCs). They progress through ring, trophozoite, and schizont stages over an approximately 48-hour period in the

intraerythrocytic developmental cycle. At the schizont stage, the infected RBC ruptures and releases 16 to 32 daughter merozoites that reinvade into new erythrocytes with an exponential cycle of infection (Figure 2).[6] Some of the intraerythrocytic parasites develop sexually and differentiate into male and female gametocytes that are taken up by a subsequent mosquito blood meal. They fertilize and sporulate in the mosquito midgut and complete the transmission cycle. The asexual cycle triggers periodic fever and, in severe cases, leads to profound anemia, organ dysfunction, and death.

Malaria is clinically classified as uncomplicated or severe based on the symptoms presenting. Uncomplicated malaria is characterized by non-specific, flu-like symptoms such as fever, chills, headaches, fatigue, and muscle aches.[1,7] Severe malaria (SM) is diagnosed by the emergence of life-threatening complications including impaired consciousness, severe anemia (low hemoglobin: <5 g/dL in children, <7 g/dL in adults or low hematocrit: <15% in children, <20% in adults)[46], metabolic acidosis, respiratory distress, renal failure, hypoglycemia, and hyperparasitemia.[7] The two most lethal manifestations of SM are severe malarial anemia (SMA) and cerebral malaria (CM). SMA is characterized by systemic hypoxia resulting from massive hemolysis and dyserythropoiesis.[8] CM is characterized by the sequestration of parasitized erythrocytes in the brain microvasculature. It typically has a fatality rate that is 2 to 5 times higher than SMA and often results in long-term neurological deficits among survivors.[8] If SM is left untreated, it has a fatality rate of about 90%.[7]

1.3 Treatment and Rising Threat of Artemisinin Resistance

Malaria control has historically relied on both vector control and antimalarial chemotherapy. In the past two decades, Insecticide-treated bed nets (ITNs) and indoor

residual spraying (IRS) have been effective in reducing malaria incidence and served as the primary means for vector control.[9] However, the emergence of insecticide resistance in mosquito populations and declining funding for these interventions threaten these efforts in malaria control.[10]

Artemisinin-based combination therapies (ACTs) have served as the first-line therapeutic treatment for uncomplicated malaria since the early 2000s due to their rapid parasite clearance and high efficacy.[11] Artemisinin derivatives can reduce parasite biomass by 10,000-fold within a single 48-hour intraerythrocytic cycle.[11] However, in 2008, the emergence and spread of artemisinin partial resistance (ART-R) was first documented in Southeast Asia, which is threatening the global malaria control.[12]

The ART-R phenotype is caused by mutations in the Kelch13 (K13) gene and manifests as delayed parasite clearance after treatment. Historically, the mutation resistance to chloroquine and sulfadoxine-purimethamine were imported from South Asia; however, the genomic surveillance has now identified at least six distinct K13 mutations which emerged in East Africa independently.[11]

Models from a clinical efficacy review predict that artemisinin resistance could lead to over 100,000 additional deaths per year.[11] The intravenous artesunate monotherapy with a full ACT course, the standard treatment for SM, is particularly vulnerable to the artemisinin resistance as it accelerates the selection of resistant parasites.[11] Therefore, the development of new interventions using novel mechanisms is desperately needed before ART-R becomes widespread across Africa.

1.4 Current Malaria Vaccine Candidates

The development of an effective malaria vaccine has been a goal of global health researchers for over a century, yet progress has been remarkably slow given the parasite's complex biology and immune evasion strategies. Currently, there are two WHO-approved vaccines targeted for malaria, RTS,S/AS01 (Mosquirix) and R21/Matrix-M. Both vaccines are pre-erythrocytic and target the circumsporozoite protein (CSP) on the surface of sporozoites to prevent hepatocyte invasion.[13,14] RTS,S showed approximately 56% efficacy against clinical malaria over a 12-month period in children between 5-17 months; however, the efficacy substantially declines over subsequent years, dropping to approximately 30% efficacy against SM.[13] R21/Matrix-M has shown improved efficacy of approximately 75% against clinical malaria in seasonal transmission settings over one year, but its protection against SM remains incompletely characterized.[14]

Since both vaccines only target the pre-erythrocytic stage, they do not induce protective immune responses against the blood-stage parasites that cause clinical symptoms and death. The development of a blood-stage vaccine has been further restricted by high antigenic polymorphism in candidate antigens such as AMA1 and MSP1.[15,16] Therefore, there is a critical need for blood-stage vaccine candidates that can complement the existing pre-erythrocytic vaccines and protect directly against SM.

Malaria vaccine candidates can usually be categorized by the parasite life-cycle stage they target (Figure 3).[17] Pre-erythrocytic vaccines (PEV) aim to prevent establishment of blood-stage infections by targeting sporozoites or liver-stage parasites. Both subunit vaccines such as RTS,S/AS01E and R21 and whole sporozoite vaccines such as PfSPZ Vaccine and

chemoprophylaxis vaccination are PEV.[17] Transmission-blocking vaccines (TBV) targeting sexual-stage antigens such as Pfs25, Pfs230, and Pfs48/45 aim to interrupt the parasite's cycle of transmission via the mosquito vector, rather than directly protecting the vaccinated individual.[17]

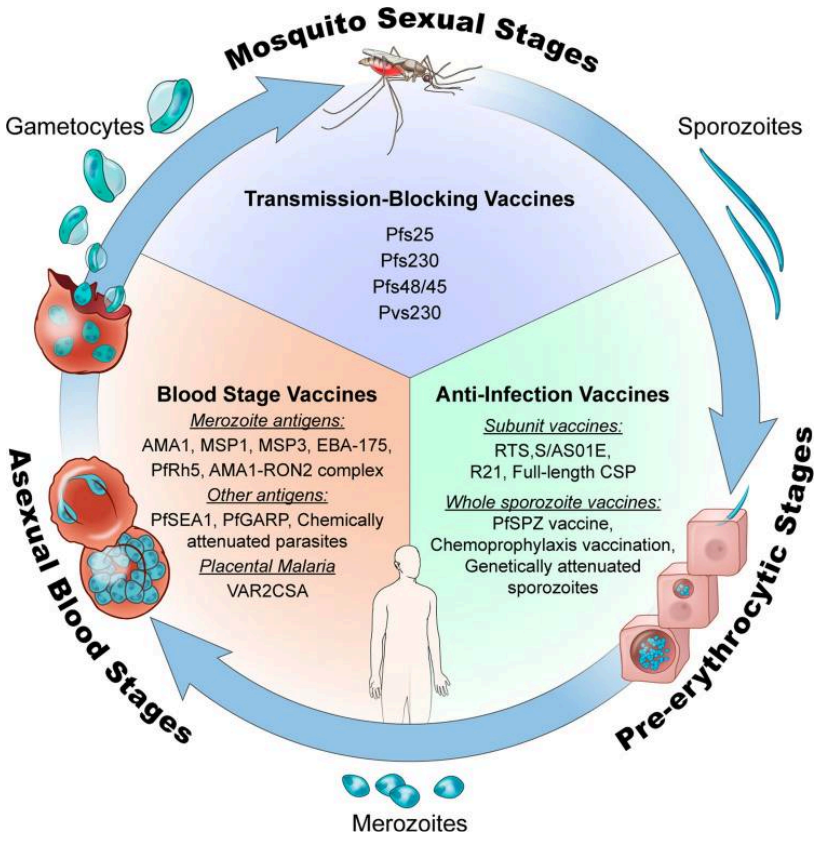

Figure 3. Life cycle stages of *Plasmodium* and vaccine candidates. Anti-infection vaccines (pre-erythrocytic) include subunit vaccines such as RTS,S/AS01E and R21, as well as whole sporozoite approaches. Adapted from Duffy and Gorres.[17]

Blood-stage vaccines (BSV) target the asexual erythrocytic parasites that are responsible for all clinical malaria (Figure 3). BSV candidates used to focus on merozoite surface antigens that involved in erythrocyte invasion, such as AMA1, MSP1, MSP3, EBA-175, and the AMA1-RON2 complex.[17] However, the clinical trials of AMA1- and MSP1-based vaccines have proved limited efficacy, primarily due to extensive antigenic polymorphism that enabled immune

evasion and insufficient induction of functional antibody titers.[15,16] More recently, PfRh5 has emerged as a leading blood-stage candidate. It is a conserved ligand that binds to the host receptor basigin and exhibits limited antigenic polymorphism. Phase 1/2b clinical trials have shown the induction of strain-transcending functional antibodies in humans.[17,18] Advances in antigen discovery and vaccine platforms (mRNA and viral vectors) have reignited the interests in the BSV field and offer the potential to overcome the limitations of earlier pre-erythrocytic vaccine strategies and to provide direct protection against severe disease.[17]

1.5 Naturally Acquired Immunity and Whole Proteome Differential Screening

Immunity to SM develops rapidly, often after one or two episodes in the malaria-endemic regions. However, immunity to uncomplicated malaria requires prolonged cumulative exposures.[19,20] Interestingly, natural acquired resistance to SM is not correlated with improved control of parasite density, which suggests that the protective antibodies target a specific and limited set of parasite antigens.[20] Our aim was to identify immunological targets that are expressed during the recovery/convalescent phase in children with SM and that may contribute to long-term protection. To this end, we collected serum/plasma samples both before and after SM episodes.

The Kurtis Laboratory at the Center for International Health Research (CIHR) at Brown University developed Whole Proteome Differential Screening (WPDS) to implement this strategy.[21,22] WPDS utilizes differential biopanning of a *P. falciparum* 3D7 blood-stage cDNA expression library displayed on T7 phage, probed with pooled serum/plasma samples collected both before and after SM episodes from children of our Kenyan longitudinal cohort study (enrollment age range 3–7 years). Through iterative rounds of positive and negative selection,

WPDS identifies parasite proteins whose epitopes are uniquely recognized by antibodies from SM children who have experienced SM episodes.[21,22]

WPDS has successfully led to the discovery of three transformative vaccine candidates: PfSEA-1, PfGARP, and PfGBP130. PfSEA-1 is a 244-kDa schizont antigen whose antibodies block parasite egress from RBCs.[21] PfGARP is an 80-kDa trophozoite surface antigen whose antibodies kill parasites by inducing programmed cell death.[22] PfGBP130 is an invasion-blocking target currently being advanced as a lipid-encapsulated mRNA vaccine.[23] Each candidate was validated through functional assays and epidemiological analyses across multiple cohorts, with PfGARP representing the first demonstration that an antibody binding to a surface-exposed blood-stage antigen can induce parasite programmed cell death.

1.6 Study Rationale and Experimental Objectives for P113

In Kurtis Lab, WPDS was adapted to identify targets from SM screening. Among the antigens identified, P113 (PF3D7_1420700) was selected as the lead candidate. P113 is a GPI-anchored merozoite surface protein (~113 kDa) encoded on chromosome 14 and highly conserved for all human-infecting Plasmodium species.[24,25]

P113 serves as the membrane anchor for Reticulocyte Binding Protein Homolog 5 (PfRh5) on the merozoite surface.[24,25] PfRh5 interacts with the host receptor basigin (CD147) on erythrocytes that are essential for invasion across all strains.[27,28] The N-terminal region binds directly to P113 and forms a releasable tether that positions the PfRh5–PfRipr–PfCyRPA invasion complex at the merozoite surface.[25,29] Antibodies targeting the PfRh5 complex inhibit erythrocyte invasion and are in advanced clinical development.[27,30]

Given that blood-stage vaccine responses depend on antibody magnitude and epitope specificity, and that antibodies to the same antigen can differ functionally with only some recognizing invasion-blocking epitopes, linear epitope mapping provides a powerful approach to pinpoint inhibitory epitopes using high-density peptide arrays. These insights can subsequently inform the rational design of minimal peptide-based vaccines.[33,34,35,36] Therefore, the goal of this thesis is to functionally validate and characterize P113 by focusing on three aims.

Aim 1: Utilize WPDS to screen potential acquired antibody targets.

Aim 2: Validate the hit and synthesized recombinant protein *in vitro*.

Aim 3: Demonstrate that anti-P113 antibodies inhibit parasite growth and characterize the inhibitory response.

Chapter 2: Methods

2.1 Study Design

This study drew on plasma samples from a prospective longitudinal cohort of 400 children living in an area of intense malaria transmission in Kenya, who were followed for three years.[21,22] Demographic and clinical variables for the cohort are summarized in Table 1. While age- and location-matched children who remained free of SM over the study period served as resistant controls (n = 391), baseline parasitemia appeared more than 3-folds higher in the SM group (398.86 vs. 123.02 per 200 WBC). Paired plasma samples were collected from each SM case at two time points: a pre-severe malaria (pre-SM) sample drawn before the severe episode and a post-severe malaria (post-SM) sample collected after the episode. The timing of these paired samples is detailed in Supp Table S2. The interval between pre- and post-SM collection ranged from approximately 41 to 102 days. This temporal pairing is thereby key to the WPDS approach. By subtracting antibody reactivities present in the pre-SM sample (baseline) from those in the post-SM sample (post-episode), we specifically isolated antigens that were differentially recognized as a consequence of the severe malaria experience, rather than from prior asymptomatic exposures.

Table 1. Characteristics of serum for susceptible screens. Demographic and clinical characteristics of children with severe malaria (SM) and non-severe malaria (non-SM) from the Kenyan longitudinal study cohort. Baseline parasitemia was determined by thick blood smear at enrollment.

Variables	SM	non-SM
Count (n=)	7	391
Age by median (range, years old)	2 (2-6)	4 (2-7)
Sex (% female)	28.57	50.13
Baseline parasitemia (per 200 WBC)	398.86	123.02
Baseline parasitemia (per uL whole blood)	5.98	1.58
Median parasite density overtime (per uL whole blood)	11.11	9.79

2.2 Whole Proteome Differential Screening

To identify novel malaria vaccine candidates, we performed differential biopanning using a blood-stage cDNA library of *Plasmodium falciparum* 3D7 strain constructed in T7 phage. Plasma samples were pooled from children aged two to five years, before and after severe malaria from our Kenyan birth cohort study.[21, 22, 24] The T7 phage display platform uses bacteriophage T7 to display peptides or proteins on the surface of the phage particle via the 10B capsid protein. Unlike filamentous phage systems, T7 assembles in the *E. coli* cytoplasm and mature phage are released by cell lysis, eliminating the requirement for secretion through the cell membrane.[38] T7 phage are extremely robust and stable to harsh conditions, including the 5 M NaCl elution used in biopanning, making them well suited for iterative selection procedures. A *P. falciparum* 3D7 blood-stage cDNA library was constructed in the T7Select vector and screened

against pooled plasma from the cohort described in Section 2.1. A schematic overview of the WPDS biopanning workflow is presented in Figure 4.

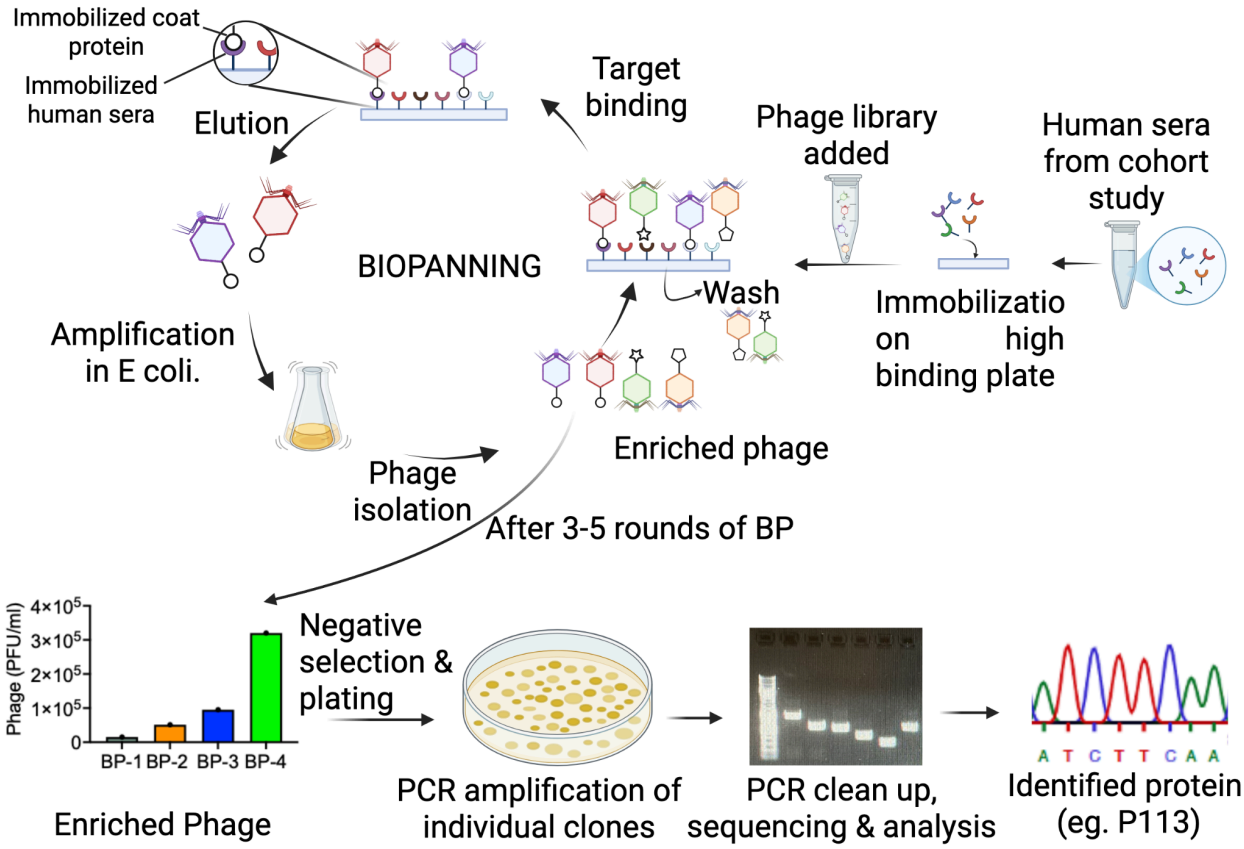

Figure 4. Overview of the whole proteome differential screening (WPDS). Human sera from the cohort study are immobilized on high-binding ELISA plates. The T7 phage-displayed *P. falciparum* cDNA library is added, and phage that bind to antibodies in sera are retained (positive selection). Bound phages are eluted, amplified in *E. coli*, and subjected to iterative rounds of biopanning (3–5 rounds). After positive selection, a single round of negative selection depletes phage recognized by susceptible sera. Enriched clones are plated, picked, PCR-amplified, and sequenced to identify candidate antigens (e.g., P113). Created with BioRender.com.

Biopanning was performed based on the T7 Phage Display system.[38] Immulon 4HBX ELISA plates (Thermo Fisher Scientific) were coated with 50 µL of a 1:100 dilution of pooled serum from children who were susceptible to severe malaria. Plates were sealed with plastic wrap and incubated at 4°C overnight to allow antibody binding to the plate surface. The following day, unbound serum was removed and wells were washed 10 times with 1× TBST (10 mM Tris-HCl, 150 mM NaCl, 0.05% Tween-20) at 1-minute intervals. Wells were then blocked with 300 µL of 5% BSA in TBST for 2 hours at room temperature, followed by an additional 10 washes with TBST.

Phage from the *P. falciparum* 3D7 cDNA library at 1×10^8 pfu were added and incubated for 2 hours at room temperature to allow binding of phage-displayed parasite proteins to immobilized antibodies. Wells were washed 10 times with 1× TBST (10 mM Tris-HCl, 150 mM NaCl, 0.05% Tween-20) to remove unbound phage. Phages were eluted with 50 µL of 5 M NaCl after 20 minutes of gentle shaking at room temperature. The eluted phage were collected by pipetting and amplified by adding 50 µL of eluted phage to 10 mL of BLT5403 *E. coli* at an optical density (OD_{600}) of 0.8 on a shaker at 37°C until bacterial lysis was observed. T7 phage replicate rapidly, with plaques forming within 3 hours and cultures lysing 1–2 hours after infection.[38] If lysis was not observed within 3 hours, the culture was diluted 1:2 with fresh media and incubation continued. Lysis was confirmed by observing thread-like structures by the naked eye and measuring OD at 600 nm. Amplified phage were isolated by centrifugation at 10,000 × g for 10 minutes at 4°C. The supernatant was collected, filtered through a 0.2 µm filter, and stored at 4°C.

To titer phage, the eluted phage were serially diluted and 0.1 mL of diluted phage was combined with 0.2 mL of BLT5403 bacteria (OD_{600} = 1.0) and 3 mL of top agar (50°C), then

poured evenly onto agar plates containing carbenicillin (50 μg/mL). Each phage plaque on the bacterial lawn encodes a parasite DNA insert that encodes a parasite protein. Through biopanning, we selected for phage recognized by antibodies in the target sera. Plaques were counted and phage titer was calculated as:

$$pfu/mL = \frac{number\ of\ plaques\ counted}{volume\ used \times dilution\ factor} \quad \text{---------- } \textit{(Formula 1)}$$

For subsequent rounds of biopanning amplification, 50 μL of phage from the previous round was used as input and the binding, washing, elution, and amplification steps were repeated. Four rounds of positive selection biopanning were performed. Phage titer increased with each successive round, from approximately 2×10^4 pfu/mL after round 1 to over 3×10^5 pfu/mL by round 4.

Negative selection was performed after three or four rounds of enrichment. For negative selection, phages were diluted to 10^5/mL and Immulon 4HB ELISA wells were coated with Pre-SM sera (1:100) overnight at 4°C. The next day, wells were washed 10 times with TBST and blocked with 300 μL of 2% BSA in TBST for 1 hour at room temperature, followed by 10 washes with TBST. Diluted phages (50,000 total) were incubated in wells for 1 hour, and unbound phages were transferred to fresh wells for five successive rounds to eliminate clones reactive to Pre-SM plasma. Unbound phage from the fifth well, which represents clones preferentially recognized by post-SM were serially diluted and plated using 0.1 mL of diluted phage with 0.2 mL of bacteria (OD_{600} = 1.0) and 3 mL of top agar, spread onto agar plates, and incubated overnight at room temperature. Plaques were counted as previously described. Following negative selection, 188 plaques were picked, and cDNA inserts were amplified by PCR using vector-specific primers T7SelectUP (5′-GGAGCTGTCGTATTCCAGTC-3′) and

T7SelectDOWN (5′-AACCCCTCAAGACCCGTTTA-3′). PCR products were sequenced for clone identification.

2.3 PCR Amplification and Sequencing

Individual phage plaques were picked from the negative selection plates and each placed in 50 µL of nuclease-free water in a 96-well PCR plate with two negative controls on each plate. Samples were denatured at 99°C for 10 minutes to release phage DNA, and 2 µL of each sample was used as template for PCR amplification. PCR was performed using the T7SelectUP and T7SelectDOWN primers (Novagen) flanking the multiple cloning site of the T7Select vector.[38] Each 50 µL reaction contained 2 µL phage lysate, 5 µL 10× NovaTaq Buffer with $MgCl_2$, 1 µL each primer (5 pmol/µL), 1 µL dNTP mix (10 mM each), and 1.25 U NovaTaq DNA polymerase. The method for PCR includes initial denaturation at 94°C (2 min) followed by 30 cycles of 94°C for 50 seconds, 55°C for 1 minute, and 72°C for 1 minute, with a final extension at 72°C for 6 minutes. PCR products were purified using the ZR-96 DNA Clean-Up Kit (Zymo Research, Cat# D4017).

Agarose gel electrophoresis was performed to confirm the presence and size of amplified inserts. Agarose gels (1%) were prepared by dissolving 0.5 g agarose in 50 mL Tris-acetate-EDTA (TAE) buffer via microwave heating (1 minute 30 seconds) until a clear solution was obtained. SYBR Green (1.5 µL) was added, and the solution was poured into a gel tray and allowed to solidify for 30 minutes. A 1 Kb DNA ladder and a 100 bp–10 Kb ladder were loaded on opposite ends of the gel, and 5 µL of each PCR product was loaded into individual wells. Electrophoresis was run at 110 V for 20 minutes in the TAE buffer, and gels were imaged

under BioRad gel documentation system. Purified PCR products were verified by agarose gel electrophoresis and subsequently submitted to Eurofins Genomics for Sanger sequencing.

2.4 Bioinformatic Analysis and Candidate Selection

Returned sequences were analyzed by nucleotide BLAST on the NCBI database (blast.ncbi.nlm.nih.gov) using the Megablast algorithm under the *P. falciparum* 3D7 species reference genome.[40] The resulting gene identities were cross-referenced on PlasmoDB (plasmodb.org)[39] to characterize each candidate antigen, including molecular weight, predicted signal peptide (SignalP)[43], predicted transmembrane domains (TMHMM), and protein length. In total, 188 plaques were analyzed across the three screens, identifying 46 differentially recognized proteins. Candidate antigens were prioritized based on predicted surface expression, molecular weight, sequence conservation, and known roles in host–parasite interactions. P113 (PF3D7_1420700) emerged as a one of the top hits across multiple screens, with a molecular weight of ~113 kDa, a predicted signal peptide, and predicted GPI anchoring to the merozoite surface.[25]

2.5 Plasmid Acquisition and Preparation

Following identification of P113 as a hit WPDS candidate, expression and purification were performed following Johnson et al. (2024) with slight modifications. The full-length ORF of P113 (969 amino acids) was codon-optimized and cloned into pD2610-v6 vector (Atum), incorporating an N-terminal secretion signal from pHL-sec and a C-terminal 10 × His-tag. Endotoxin-free plasmid DNA was prepared using the Qiagen Plasmid Maxi Kit and verified by

Sanger sequencing (Eurofins Genomics). Insert identity was confirmed by Megablast alignment to the *P. falciparum* 3D7 reference genome on PlasmoDB.[39,40]

2.6 Recombinant Protein Expression

Recombinant P113 (rP113) was expressed in HEK293 mammalian cells using Lipofectamine (Invitrogen) (Figure 5). This is a mammalian expression platform that supports proper folding, disulfide bond formation, and glycosylation of complex eukaryotic proteins. HEK293 cells were maintained at 37°C in a humidified atmosphere with 5% CO_2 on an orbital shaker (125 rpm). Cells were passed every 3–4 days and used for transfection when viability exceeded 95%. Endotoxin-free plasmid was transfected into HEK293 cells, and culture supernatant was harvested on day 5.

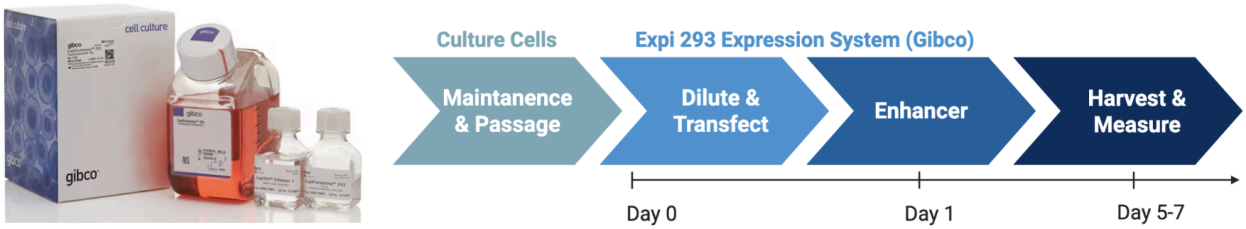

Figure 5. Recombinant P113 expression and purification pipeline. Expi293F cells were maintained in culture, diluted and transfected with the codon-optimized P113 plasmid on Day 0, supplemented with enhancers on Day 1, and harvested at Days 5–7.

On the day of transfection (Day 0), cells were diluted to ~3 × 10^6 cells/mL in fresh medium. Plasmid DNA was complexed with ExpiFectamine™ 293 Reagent in Opti-MEM I and added to the culture. At ~18 hours post-transfection, ExpiFectamine 293 Transfection Enhancers

1 and 2 were added per the manufacturer's protocol. Expression was monitored by SDS-PAGE and Western blot using anti-10 x His antibody (Abcam ab18184). Supernatants were harvested 5–7 days post-transfection by centrifugation (3,000 × g, 20 min) and 0.2 μm filtration.

Expression was confirmed in post-transfection samples by SDS-PAGE and Western blot using anti-His antibody, with rP113 absent from pre-transfection controls. Following verification by mass spectrometry, the identity and integrity of the protein was confirmed with the expected sequence.

2.7 Protein Purification

His-tagged P113 was purified from clarified supernatant using a FineLine Pilot 35 system (GE Healthcare) equipped with a 150 mL Ni-NTA column via nickel affinity chromatography. The binding buffer is utilized after equilibration (50 mM sodium phosphate, 300 mM NaCl, 10 mM imidazole, pH 8.0). The clarified supernatant was loaded at 1 mL/min. The column was washed with 10 column volumes of wash buffer containing 20 mM imidazole. Bound proteins were eluted stepwise with 100 mM, 200 mM, and 500 mM imidazole. Elution fractions were run and assessed by SDS-PAGE on BioRad Mini-PROTEAN TGX gels (250 V, 19 min) individually and Western blot using Alkaline Phosphatase Anti-6X His tag® antibody [HIS-1] (Abcam, ab49746). The membrane was then developed with BCIP®/NBT substrate (Millipore Sigma, B5655-5TAB). There were two distinct bands observed, consistent with the predicted ~113 kDa molecular weight and a potential cleavage product. Both bands were confirmed as P113 (PF3D7_1420700) by LC-MS/MS mass spectrometry following in-gel trypsin digestion.[25] Purified rP113 was buffer exchanged into 10 mM sodium phosphate, 0.05% Tween-20, and 3% sucrose by tangential flow ultrafiltration (50 cm^2 filter, 5 kDa cutoff, Pall). Protein was

concentrated to 500 µg/mL, lyophilized, and sealed under nitrogen to be quantified by BCA assay and further use.

2.8 Mouse Immunization and Serum Collection

Mouse antisera were generated via immunization with recombinant protein and plasmid DNA as previously described.[21] For protein immunization, 50 µg of purified rP113 was emulsified in equal volume of TiterMax Gold adjuvant (Sigma) and injected intraperitoneally at 2-week intervals for four doses (days 0, 14, 28, 42). For DNA immunization, endotoxin-free plasmid was injected intramuscularly (50 µg per dose) every 3 weeks for four doses. Control mice received adjuvant-only (protein) or PBS (DNA). BALB/cJ mice were used for all immunizations. An initial study cohort of 5 mice per group was followed by a subsequent expansion to 45 total immunized mice to confirm the ~20% responder rate (Figure 6).

At the end of the immunization schedule, mice were sacrificed by terminal cardiac puncture under anesthesia. Blood was carefully collected to prevent blood lysis and allowed to clot. The serum was separated by centrifugation, heat-inactivated at 56°C for 30 minutes. Uninfected human O+ erythrocytes were added and the sera were pre-absorbed to remove any complement proteins mediated responses. Processed sera were aliquoted and stored at -80°C until use. Anti-P113 antibody titers were confirmed by ELISA. All animal procedures were approved by the Brown University Institutional Animal Care and Use Committee (IACUC).[27]

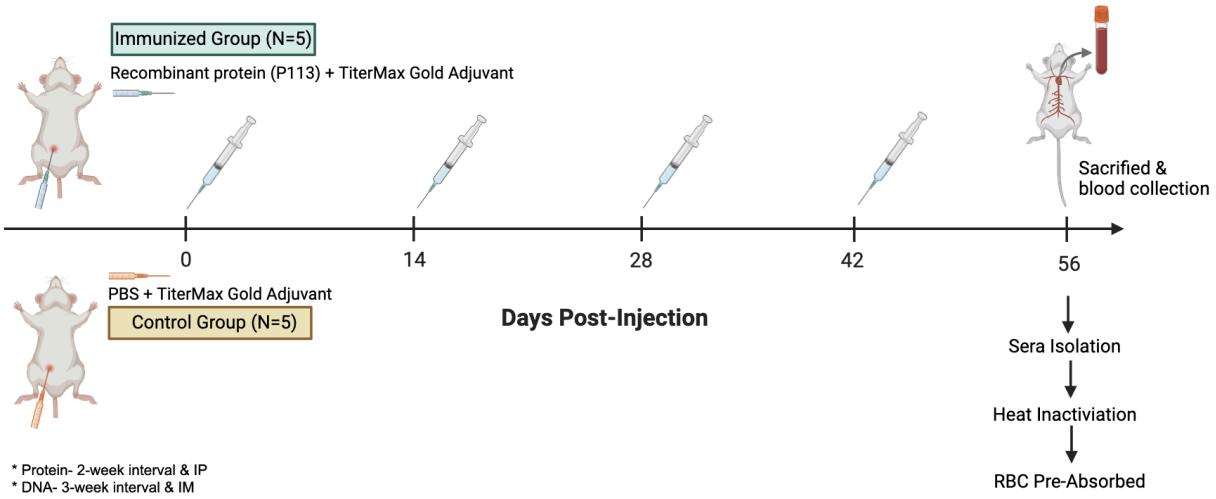

Figure 6. Mouse immunization schedule and serum processing. Five BALB/c mice per group received four biweekly intraperitoneal immunizations (days 0, 14, 28, 42) with rP113 + TiterMax Gold Adjuvant (immunized group, N=5) or PBS + TiterMax Gold (control group, N=5). Terminal blood collection was performed on day 42 by cardiac puncture. Sera were isolated, heat-inactivated, and pre-absorbed against human RBCs prior to functional assays. Created with BioRender.com.

2.9 Growth Inhibition Assay

P. falciparum 3D7 asexual blood-stage parasites (3D7 strain) were cultured following Trager and Jensen (1976) with minor modifications.[41] Cultures were maintained in RPMI 1640 medium containing 25 mM HEPES, 5% human O+ erythrocytes, 5% Albumax II (Invitrogen), 24 mM sodium bicarbonate, and 10 µg/mL gentamicin at 37°C in a gas mixture of 5% CO_2, 1% O_2, and 94% N_2.[41,44]

Growth inhibition assays (GIAs) were performed using polyclonal antisera from both recombinant protein and DNA-based immunizations.[33] Negative controls included adjuvant-only sera (for protein immunizations) and PBS-immunized sera (for plasmid) from BALB/cJ mice.

All test sera were heat-inactivated at 56°C for 30 minutes and pre-incubated with human RBCs for 1 hour before use at a final concentration of 10%. Parasites (3D7) were synchronized to the ring stage in two rounds by sorbitol lysis. Two days before the GIA, cultures were synchronized twice with 5% D-sorbitol and the parasitemia was maintained < 4% throughout two replication cycles (96 hours). The second round of synchronization was performed at the ring stage one replication cycle before the assay so that the majority of parasites were at the ring stage at the start of the assay and assessed by flow cytometry and CellaVision.

Synchronized *P. falciparum* 3D7 parasites were prepared at the ring stage and adjusted to 0.4% parasitemia and 1% hematocrit in the complete RPMI medium. For each assay, 100 µL of parasite suspension was added to wells of a 96-well plate. Cultures were performed in triplicate with three biological replicates. Plates were incubated for approximately one full erythrocytic cycle (up to 72 hours) at 37°C in a controlled gas mixture (5% CO_2, 1% O_2, 94% N_2).

Following the incubation period, parasitemia was quantified by flow cytometry and CellaVision. For flow cytometry, aliquots were transferred into a new plate (flow plate) and stained with 4 µM Hoechst nuclear staining solution in PBS and allowed to stain for 30 minutes in dark. The aliquots were washed with PBS three times with centrifuging (800 RCF, 5 minutes each) before being read by flow cytometry. Fluorescence at 450 nm was measured with a CytoFLEX (Beckman Coulter) flow cytometer with acquisition of 150,000 erythrocytes events per sample, gating on Hoechst-positive events to distinguish infected from uninfected erythrocytes. Since mature erythrocytes lack DNA and only iRBCs fluoresce, the parasitemia would also be analyzed by CellaVision DM9600 with Giemsa-stained thin smears for AI counting and manual selecting verification. Samples were tested in duplicate in each experiment,

and three independent experiments were performed. The parasitemia values were exported to GraphPad Prism and percent inhibition was calculated as:

$$\%\ Growth\ Inhibition\ =\ (1\ -\ \frac{Test\ parasitemia - RBC\ Control}{iRBC\ Control - RBC\ Control})\ \times\ 100 \quad \text{---- } \textit{(Formula 2)}$$

2.10 Antibody Titer

P113-specific antibody titers were quantified using a bead-based multiplex immunoassay on the Bio-Plex Luminex xMAP platform, as previously described.[22] Recombinant P113 was covalently coupled to carboxylated magnetic microspheres (MagPlex beads, Luminex) using the Bio-Plex Amine Coupling Kit according to the manufacturer's instructions. Beads were activated with sulfo-NHS and EDC, and purified rP113 was conjugated at a concentration optimized to achieve saturating antigen density. BSA-coupled beads served as a negative control to measure non-specific binding.

For each assay, 50 µL of diluted mouse serum was incubated with 50 µL of the P113-coupled bead mixture in a 96-well plate. Plates were sealed with plastic wrap, protected from light, and shaken at 300 rpm for 2 hours at room temperature. After incubation, wells were washed three times with 1 × wash buffer, and a biotinylated anti-mouse IgG detection antibody was added. Plates were incubated for 1 hour at room temperature with shaking, washed again, and subsequently incubated with streptavidin–phycoerythrin (SA-PE) reporter conjugate for 30 minutes. Following final washes, beads were resuspended in 125 µL of assay buffer and immediately analyzed on a Bio-Plex 200 system (Bio-Rad) operated with Luminex xMAP technology. A minimum of 50 beads per analyte were acquired per well. Median fluorescence

intensity (MFI) values were recorded and corrected by subtracting the MFI of BSA-coupled control beads.

Sera from all P113-immunized mice were tested at serial dilutions of two-fold, and antibody concentrations were compared between growth-inhibitory and non-inhibitory sera to determine whether functional heterogeneity reflected differences in antibody abundance. Titers at the end point were defined as the highest dilution yielding a corrected MFI exceeding the mean plus three standard deviations of naïve control sera.

2.11 Western Blot Analysis of Native Parasite P113

To confirm that anti-P113 antibodies recognize the native parasite-expressed protein, synchronized late trophozoite/schizont stage *P. falciparum* 3D7 were cultured and the iRBCs were harvested by centrifugation. Parasite pellets were isolated by selective lysis of erythrocyte membranes with 0.05% saponin in PBS on ice for 10 minutes, followed by three washes in ice-cold PBS containing EDTA-free protease inhibitor cocktail (PIC; Roche) to prevent protein degradation during processing.

Parasite pellets were solubilized in a sodium dodecyl sulfate (SDS) reducing sample buffer (Invitrogen), boiled at 95°C for 7 minutes to fully denature proteins, and briefly centrifuged to remove insoluble debris. Denatured samples were loaded onto 4–12% Bis-Tris precast polyacrylamide gels (BioRad) alongside a pre-stained molecular weight marker. Electrophoresis was performed in the SDS running buffer at 250 V for around 20 minutes until the dye front reached the bottom of the gel.

Following electrophoresis, proteins were transferred from the gel onto nitrocellulose membranes (Roche) using a wet transfer apparatus. Transfer was performed in a Tris-glycine

transfer buffer containing 20% methanol at 100 V for 1 hour at 4°C, or overnight at 30 V. Transfer efficiency was confirmed by Ponceau S staining of the membrane.

Membranes were blocked with 5% skim milk in PBS for 1 hour at room temperature to prevent non-specific antibody binding. After blocking, membranes were probed overnight at 4°C with primary antibodies diluted in the blocking buffer. For expression confirmation, commercial anti-His tag antibody was used; for native protein detection, anti-P113 mouse immune sera (both growth-inhibitory and non-inhibitory) were used at 1:1,000 dilution to determine whether functional growth-inhibitory activity correlated with the ability to recognize native parasite P113.

Following primary antibody incubation, membranes were washed five times with PBS containing 0.1% Tween-20 (PBS-T) at 5-minute intervals. Fluorescently labeled secondary antibodies (IRDye 680RD or IRDye 800CW conjugated goat anti-mouse IgG, LI-COR Biosciences) were applied at 1:10,000 dilution for 1 hour at room temperature in the dark. Membranes were washed five times with PBS-T and imaged on a LI-COR Odyssey CLx Infrared Imaging System, which enables simultaneous two-channel fluorescence detection for multiplexed protein visualization.

Anti-β-actin antibody was included as a loading control to confirm equal protein loading across lanes for both host and parasite proteins. Recombinant unpurified P113 was loaded as a positive control to confirm antibody specificity, and lysates from untransfected HEK293 cells served as a negative control to verify the absence of non-specific cross-reactivity.[25]

2.11 Statistical Analysis

All statistical analyses were performed in GraphPad Prism. Data are presented as mean ± SEM unless otherwise stated. Group comparisons were performed using the non-parametric

two-sided Mann–Whitney *U* test, appropriate for the small sample sizes in this study. A *P*-value of less than 0.05 was considered statistically significant. Sample sizes (n = 5 per group) were based on prior immunization studies in the Kurtis Laboratory that achieved statistically significant results with similar group sizes.

Chapter 3: Results

3.1 Identification of P113

As mentioned in Section 2.2, *P. falciparum* 3D7 blood-stage cDNA expression library displayed on T7 phage was subjected to iterative differential biopanning using paired pre-CM (susceptible) and post-CM plasma samples from a Kenyan birth cohort of children who experienced severe malaria. Four rounds of positive selection against post-CM plasma were followed by a single round of negative selection against pre-CM plasma (Figure 4). Therefore, the enriched phage clones indicated antigen specifically recognized by antibodies acquired during the recovery of CM.

(a)

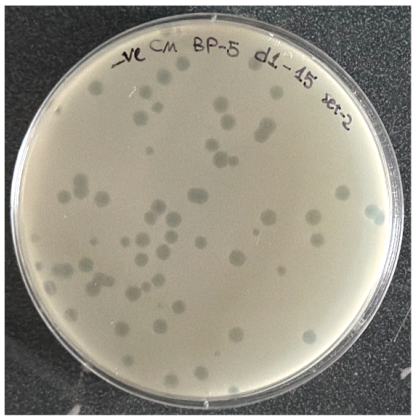

(b)

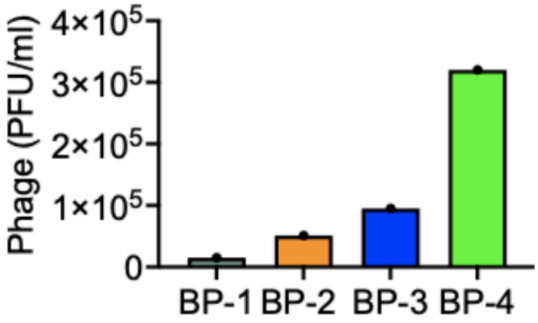

Figure 7. Biopanning amplification and phage plate. *Left (a):* Representative agar plate showing discrete plaques after negative selection. *Right (b):* Quantification of phage titers (PFU/mL) across the four rounds of biopanning (BP-1 to BP-4). Phage titers increased progressively with each round, with the largest increase observed between BP-3 and BP-4, demonstrating successful enrichment of antibody-reactive clones.

To quantify the amplification of enriched phage across the four rounds of biopanning , the phage titer (PFU/mL) was monitored by titration on BLT5403 bacterial pawns. It increased progressively from biopanning round 1 (BP-1) to round 4 (BP-4), with the heaviest enrichment

observed between BP-3 and BP-4 (Figure 7b). The final plate of phage recovered from negative selection showed a diverse collection of discrete plaques, each encoding a distinct parasite peptide fragment (Figure 7a).

A total of 188 individual plaques from the final enriched pool were randomly picked, and their displayed inserts were amplified by PCR, sequenced, and identified by Megablast alignment against the *P. falciparum* 3D7 reference genome on PlasmoDB. Sequence analysis revealed 46 differentially recognized parasite proteins. Each identified gene was characterized using PlasmoDB to confirm its molecular weight (Da), protein length (amino acids), SignalP which indicates the presence of a signal peptide directing the protein to the secretory pathway, and TMHMM which predicts transmembrane helices indicative of membrane association. The presence of a signal peptide and/or transmembrane domain suggests that the protein is surface-exposed or secreted, and therefore potentially accessible to antibody-mediated neutralization, which is a critical requirement for a vaccine candidate. A representative subset of the top hits is summarized in Table 2.

Four rounds of positive selection revealed a markedly oligoclonal response, with 34.48% of BP4 clones encoding PfGARP (PF3D7_0113000, highlighted yellow in Table 2). PfGARP is a previously validated blood-stage vaccine candidate from the Kurtis Laboratory.[22] Moreover, in order to obtain a broader repertoire, we also sequenced differentially recognized phage after three rounds of positive selection. P113 (PF3D7_1420700, highlighted yellow) showed enrichment at 2.27% in BP3 clones (Supp. Table S1). Additional hits included sortilin (PF3D7_1451800, 10.23% in BP3 in Supp. Table S1), exportin-1 (PF3D7_0302900, 21.59% in BP3; Supp. Table S1), rhoptry-associated membrane antigen (PF3D7_0707300, 2.76% in BP4; Supp. Table S1), and several exported and parasitophorous-vacuole proteins (Table 2). The

majority of the dominating candidates had either a signal peptide (SignalP) or a transmembrane domain (TMHMM), or both. This validates that our WPDS approach preferentially enriches the surface-accessible parasite proteins.

Table 2. Representative parasite proteins identified by Whole Proteome Differential Screening (WPDS). Inserts from 188 plaques recovered after differential biopanning were PCR-amplified, sequenced, and identified by Megablast alignment to the P. falciparum 3D7 genome. Gene characteristics were retrieved from PlasmoDB.

Transcript ID (Plasmodium falciparum 3D7)	Gene ID	MW (Da)	Has SignalP	TMHMM	Length (aa)
Surface protein P113	PF3D7_1420700	112,574	Yes	Yes	969
Glutamic acid-rich protein (GARP)	PF3D7_0113000	79,795	Yes	Yes	673
Sortilin	PF3D7_1451800	102,270	No	Yes	895
Conserved Plasmodium protein	PF3D7_1228700	136,557	Yes	Yes	1,135
Merozoite surface protein 4	PF3D7_0207000	30,549	No	Yes	272
Rhoptry-associated membrane antigen	PF3D7_0707300	103,641	Yes	No	861
Ring-exported protein 1	PF3D7_0935900	83,041	No	Yes	713
PRE-binding protein	PF3D7_1011800	131,626	No	No	1,139
Conserved Plasmodium protein	PF3D7_1021200	82,849	No	No	689
Exported protein 1	PF3D7_1121600	17,296	Yes	Yes	162
Conserved protein, unknown function	PF3D7_1329500	218,438	No	No	1,844
Conserved Plasmodium protein, unknown function	PF3D7_1329600	35,019	No	No	301
Plasmepsin III	PF3D7_1408100	51,693	No	Yes	451

P113 was chosen for downstream characterization due to its dominant representation in the screening. It is a strong and reproducible antibody recognition in post-CM children. Also, its predicted GPI-anchored localization on the merozoite surface is consistent with accessibility to antibody-mediated neutralization along with its low sequence variation across field isolates.

These are required for a strain-transcending vaccine. Additionally, its role in anchoring the PfRh5 invasion complex at the merozoite surface is well characterized, which also makes P113 a good candidate.

3.2 Recombinant P113

Regarding the immunogenicity studies, a codon-optimized construct encoding the P113 ectodomain with a C-terminal 10X His-tag was synthesized and was cloned into a mammalian expression vector. Then, it was transfected into suspension Expi293F cells using the ExpiFectamine 293 reagent system as discussed in Section 2.6. Culture supernatants were harvested 5–7 days post-transfection, and recombinant P113 (rP113) was purified from clarified supernatant by immobilized metal affinity chromatography (IMAC) on a nickel-charged column (Figure 8).

The Western blot results indicate that the purified protein using an anti-His tag antibody had two close but distinct immunoreactive bands. The upper band migrated in proximity to the predicted molecular weight of the full-length P113 ectodomain (112.6 kDa). However, the second band which migrated slightly faster was also consistently detected. This two-band pattern has been observed for other GPI-anchored merozoite surface proteins. This phenomenon may reflect differential N- or O-linked glycosylation of the recombinant protein in Expi293 cells as partial proteolytic processing or the presence of alternative conformational isoforms. Both bands were excised from the SDS-PAGE gel and sent to MS Bioworks for LC-MS/MS analysis to confirm their identity. Mass spectrometry analysis confirmed that both bands correspond to P113. No other parasite proteins were identified as major components of either band, which confirms the purity and identity of the recombinant preparation. The two bands are referred as

P113#1 (upper, ID 67847) and P113#2 (lower, ID 67848) according to the Mass Spec validation from MSBioworks (Supp Figure S3).

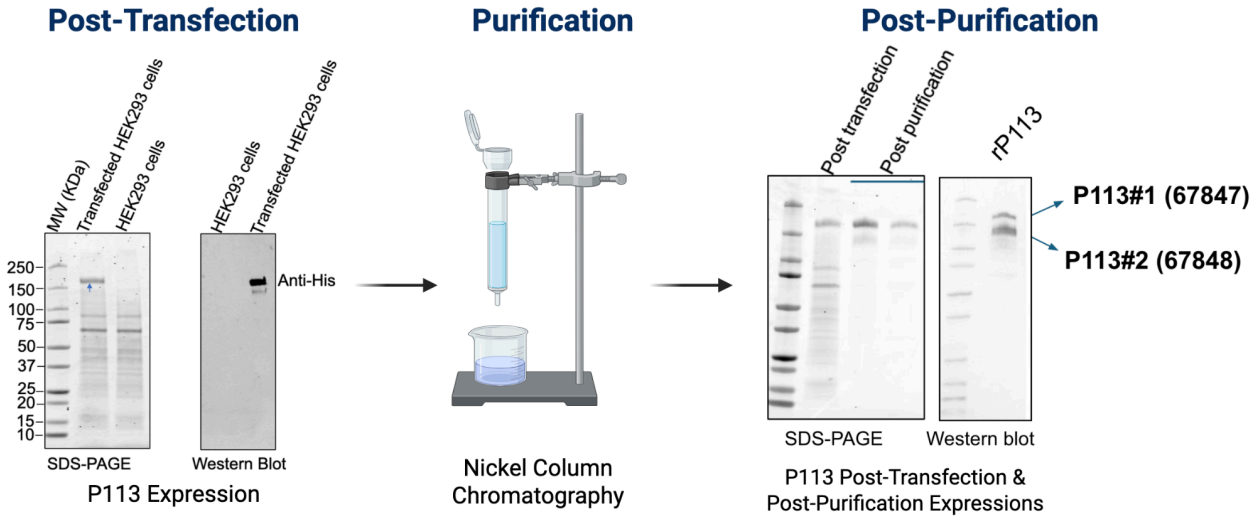

Figure 8. Recombinant P113 expression. *Left:* Post-transfection SDS-PAGE and anti-His WB of transfected vs. untransfected HEK293 cells. *Middle:* Schematic of nickel-column purification workflow. *Right:* Post-purification SDS-PAGE and WB of purified P113 revealed two distinct immunoreactive bands at approximately 113 kDa (P113#1; ID 67847) and a slightly lower molecular weight (P113#2; ID 67848).

3.3 Anti-P113 Immune Sera Inhibit P. falciparum 3D7 Growth In Vitro

As discussed in Section 2.8, mice sera were collected two weeks after the final injection and screened for growth-inhibitory activity (GIA) in an *in vitro* synchronized ring-stage 3D7 parasites. Parasitemia was quantified after approximately 72 hours of culture by Hoechst staining and flow cytometry. Only 20% of P113-immunized mice sera exhibited strong growth-inhibitory activity, which significantly reduced parasitemia compared with adjuvant-only control sera in a dose-dependent manner (Figure 9).

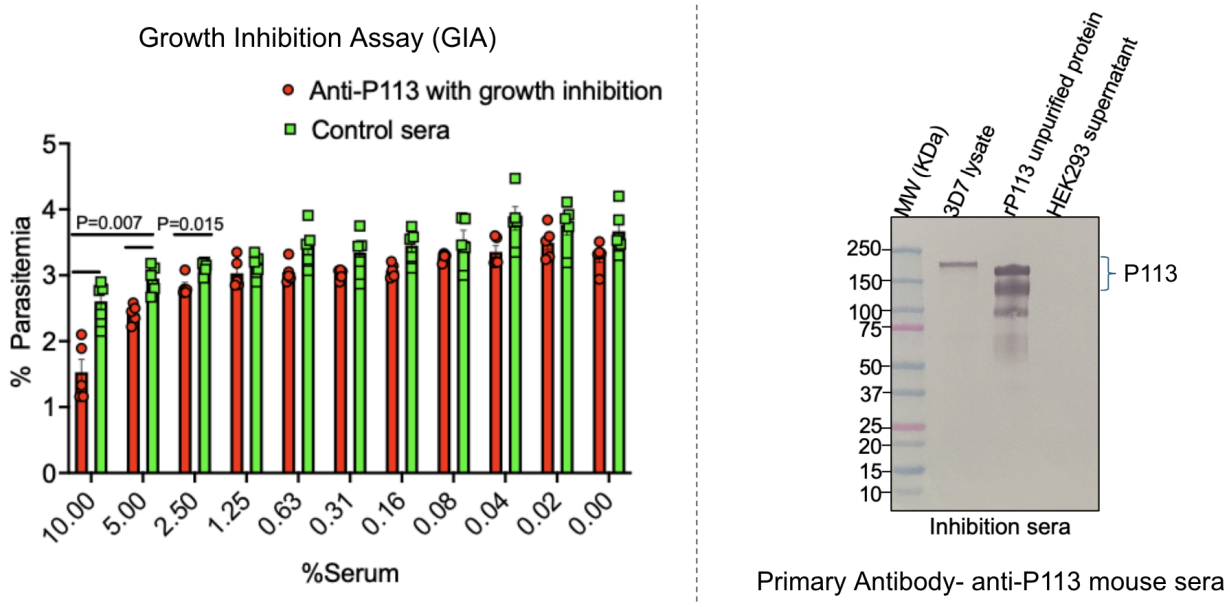

Figure 9. Anti-P113 immune sera inhibit 3D7 growth in vitro. *(Left)* GIA results. Ring-stage 3D7 parasites were cultured for ~72 h at 37 °C in the presence of serial two-fold dilutions of anti-P113 mouse sera (red) or adjuvant-only control sera (green), starting from a final concentration of 10% serum equivalent. Parasitemia was quantified by Hoechst staining. At 10% and 5% serum, anti-P113 sera produced significant reductions in parasitemia compared with adjuvant controls ($p = 0.007$ and $p = 0.015$, respectively; Mann–Whitney U test). Data points represent individual mice ($n = 5$ per group); error bars show mean ± SEM. *(Right)* WB probed with anti-P113 inhibitory mouse sera as primary antibody. The inhibitory sera recognized both native P113 in 3D7 parasite lysate and recombinant P113. HEK293 supernatant served as a negative control and showed no reactivity.

At a concentration of 10%, P113-immunized sera reduced parasitemia significantly relative to control cultures ($p = 0.007$, Mann–Whitney *U* test), while adjuvant-only sera showed no inhibitory activity. Serial two-fold dilutions of immune sera revealed concentration-dependent growth inhibition, indicating a specific antibody-mediated effect. Furthermore, Western blot analysis (Figure 9) using inhibitory mouse sera as the primary antibody demonstrated that the growth-inhibitory antibodies recognized native P113 in *P. falciparum* 3D7 lysate and rP113 in unpurified supernatant. Supporting the specificity of this response, no signal was detected in supernatant from untransfected HEK293 cells.

3.4 Growth Inhibition Is Not Determined by Antibody Titer or Antigen Recognition

Since only 20% of the P113-immunized mice produced sera with growth-inhibitory activity, we were wondering whether the difference between inhibitory and non-inhibitory sera reflected differences in antibody quantity, antigen recognition, or epitope specificity. To address this, we directly compared the inhibitory and non-inhibitory anti-P113 sera across multiple parameters (Figure 10).

As confirmed with the GIA results, the inhibitory sera produced a significant, dose-dependent reduction in parasitemia at 10% and 5% serum concentrations ($p = 0.007$ and $p = 0.015$, respectively). However, the remaining P113-immunized mice showed parasitemia levels similar to adjuvant-only controls (Figure 10a). The antibody titer analysis with serial dilution fluorescence assay demonstrated that the inhibitory and non-inhibitory sera contained similar anti-P113 antibody concentrations. As shown on Figure 10b, the titer curves for inhibitory and non-inhibitory sera are overlapping across dilutions from 1:1,000 to over 1:3,000,000 with minimal to none outlier or deviation.

Western blot analysis further confirmed that both inhibitory and non-inhibitory sera recognized native P113 in *P. falciparum* 3D7 parasite lysates at the expected molecular weight, and both recognized rP113 in unpurified supernatant (Figure 10c). Lysates from untransfected HEK293 cells served as negative controls with no reactivity. These results confirm that all P113-immunized mice generated antibodies capable of recognizing both recombinant and native parasite P113, ruling out the possibility that the non-inhibitory mice simply failed to seroconvert or produced antibodies that could not recognize the native protein.

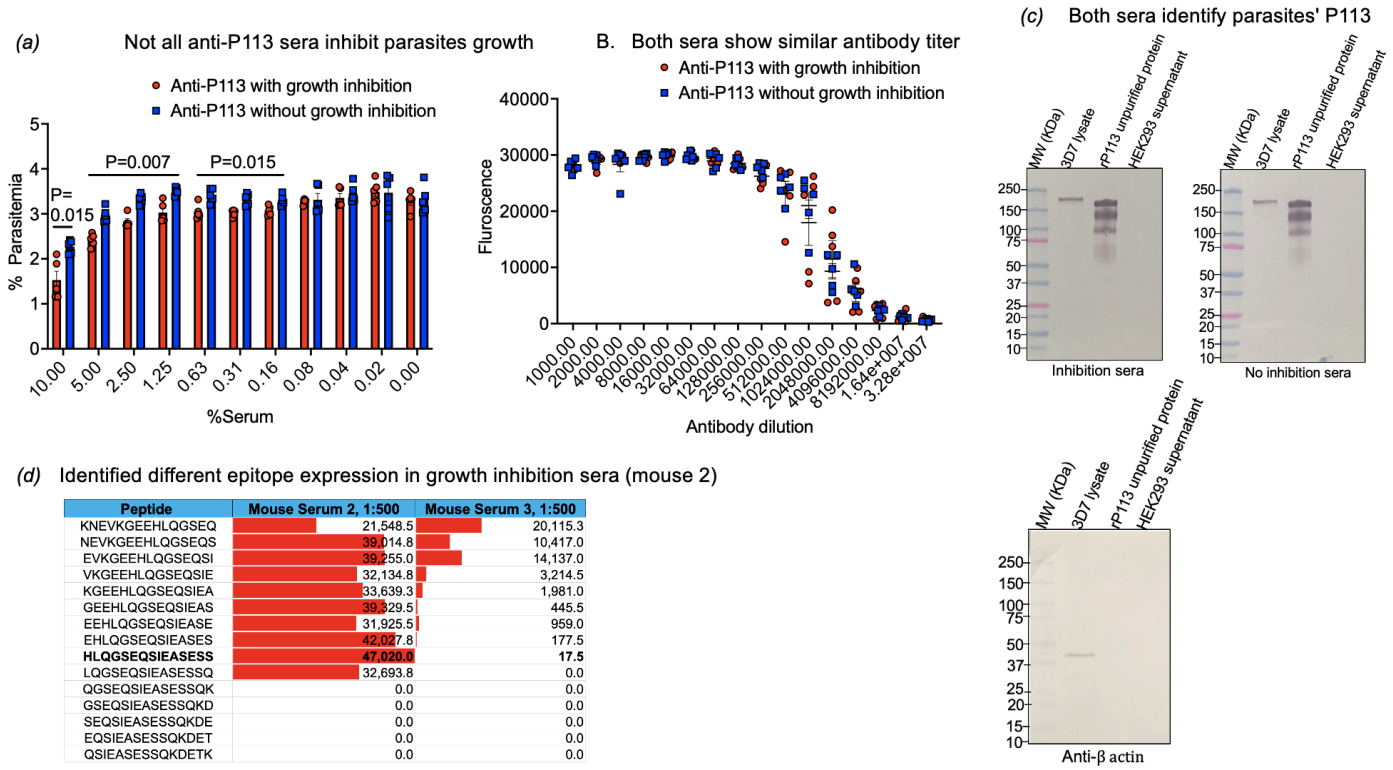

(d) Identified different epitope expression in growth inhibition sera (mouse 2)

Peptide	Mouse Serum 2, 1:500	Mouse Serum 3, 1:500
KNEVKGEEHLQGSEQ	21,548.5	20,115.3
NEVKGEEHLQGSEQS	39,014.8	10,417.0
EVKGEEHLQGSEQSI	39,255.0	14,137.0
VKGEEHLQGSEQSIE	32,134.8	3,214.5
KGEEHLQGSEQSIEA	33,639.3	1,981.0
GEEHLQGSEQSIEAS	39,329.5	445.5
EEHLQGSEQSIEASE	31,925.5	959.0
EHLQGSEQSIEASES	42,027.8	177.5
HLQGSEQSIEASESS	**47,020.0**	**17.5**
LQGSEQSIEASESSQ	32,693.8	0.0
QGSEQSIEASESSQK	0.0	0.0
GSEQSIEASESSQKD	0.0	0.0
SEQSIEASESSQKDE	0.0	0.0
EQSIEASESSQKDET	0.0	0.0
QSIEASESSQKDETK	0.0	0.0

Figure 10. Comparison of inhibitory and non-inhibitory anti-P113 sera. *(a)* Growth inhibition assays comparing anti-P113 sera with growth inhibition (red) versus anti-P113 sera without growth inhibition (blue). *(b)* Antibody titers of inhibitory and non-inhibitory sera measured by fluorescence-based assay across serial dilutions; both show comparable anti-P113 antibody concentrations. *(c)* Western blot analysis demonstrating that both inhibitory and non-inhibitory sera recognize native P113 in 3D7 parasite lysates and recombinant P113 in unpurified supernatant. Untransfected HEK293 cells served as negative controls. *(d)* PEPperMAP Linear Epitope Mapping comparing inhibitory serum (mouse 2) and non-inhibitory serum (mouse 3) at 1:500 dilution. Data are presented as mean ± SEM. Statistical significance was assessed using the Mann–Whitney *U* test.

To determine whether epitope specificity could explain the functional difference, PEPperMAP® Linear Epitope Mapping was performed with 15-mer overlapped peptides spanning the full P113 sequence (969 peptides, each 15 amino acids long with a 14-residue overlap, printed in duplicate for a total of 1,938 spots, framed by HA control peptides). Mouse 3 was chosen as a representative non-inhibitory serum (1:500 dilution). The overall binding profiles of the inhibitory serum (mouse 2, 1:500 dilution) and non inhibitory serum (mouse 3)

were broadly similar. They showed a strong polyclonal response with most prominent peaks shared between the two sera (Supp Figure S1, Supp Figure S2). Both sera recognized multiple epitopes distributed across the P113 sequence, including strong signals at epitopes DNESD, DLVLLY, VNDLEP, FRKYNPE, and several others (Supp Figure S1).

Despite these broadly similar profiles, the inhibitory serum (mouse 2) showed a distinct binding pattern to a slightly shifted epitope sequence, HLQGSEQSIEASESS (Figure 10d). This peptide exhibited the most noticeable differential response in the growth-inhibitory serum compared to the non-inhibitory serum. The observation that inhibitory and non-inhibitory sera share broadly similar overall binding profiles yet differ in their recognition of this specific epitope suggests that functional inhibition is governed not by total antibody magnitude or the breadth of epitope recognition, but rather by fine specificity for a key inhibitory epitope within P113.

Chapter 4: Discussion and Conclusion

4.1 Overview

The goal of this thesis was to identify and functionally validate a novel blood-stage vaccine candidate from among the *P. falciparum* antigens differentially recognized by antibodies acquired by children after experiencing severe malaria episodes. Using the WPDS screen, we identified P113 (PF3D7_1420700) as a potential candidate antigen. We produced recombinant protein, immunized mice, and demonstrated that a subset of immunization-induced antibodies can inhibit *P. falciparum* growth *in vitro*. Here we will discuss the significance of these findings, the mechanistic insights gained from epitope mapping, the limitations of the current study, and future directions for P113 development.

4.2 Discovery and Candidate Selection of P113

WPDS recovered 46 differentially recognized *P. falciparum* proteins from 188 sequenced phage clones (Table 2). The independent recovery of PfGARP (34.48% of BP4 clones), which is a validated vaccine candidate from the Kurtis Laboratory, served as an internal positive control and confirmed the technical robustness of the biopanning pipeline. Four rounds of positive selection indicated an oligoclonal response dominated by PfGARP (Supp Table S2). After three rounds, biopanning-sequencing revealed an expanded antigenic repertoire, with P113 accounting for 2.27% of the total BP3 clone population. (Supp Table S2).

We prioritized P113 for downstream functional assays for three main reasons:

(1) It is a 112.6-kDa GPI-anchored merozoite surface protein that anchors the PfRh5:CyRPA:Ripr invasion complex to the merozoite membrane[25,29], which is at a critical juncture in erythrocyte invasion;

(2) It shows a limited sequence variation across strains, suggesting that strain-transcending immunity may be achievable[25];

(3) Despite its role in invasion, P113 has received relatively limited attention as a vaccine target compared to PfRh5 itself. To our knowledge, this thesis provides the first demonstration that recombinant protein immunization can generate anti-P113 antibodies capable of inhibiting *P. falciparum* growth *in vitro*.

4.3 Epitope Specificity Drives Growth Inhibition

Our immunization studies showed that only ~20% of mice (out of 45 total) produced growth-inhibitory sera, even though all immunized mice seroconverted and generated comparable anti-P113 antibody titers (Figure 10b). This dissociation between seroconversion and functional inhibition may indicate that growth inhibition is determined by fine epitope specificity rather than antibody quantity. Both inhibitory and non-inhibitory sera recognize native P113 in parasite lysates and recombinant protein by Western blot (Figure 10c). However, only the inhibitory sera exhibited dose-dependent parasite growth inhibition (Figure 10a). PEPperMAP® epitope mapping also showed that the overall binding profiles of inhibitory and non-inhibitory sera were broadly similar, with a strong polyclonal response and most prominent peaks shared between the two (Supplementary Figure S1). However, the inhibitory serum uniquely recognized a shifted epitope (HLQGSEQSIEASESS). This epitope exhibited the most pronounced differential reactivity (Figure 10d). This observation suggests that functional inhibition is

controlled by fine specificity for a key inhibitory epitope within P113, not by total antibody quantity or breadth of epitope recognition.

4.4 Polyclonal Antibodies Recognize Multiple Functional Epitopes

Recent work by Campeotto et al. (2020) showed that a monoclonal antibody against P113 bound the PfRh5-P113 interface and blocked the interaction but did *not* inhibit parasite growth *in vitro*.[45] This apparent dissociation of antibody binding without functional inhibition illustrated that not all epitopes that block molecular interactions are sufficient for parasite growth inhibition. In contrast, our polyclonal sera recognize multiple epitopes on P113 and successfully inhibit growth. This suggests that naturally acquired polyclonal responses, which target diverse epitopes, may have functional inhibition through epitopes that monoclonal antibodies targeting single sites cannot achieve. The importance of targeting functional epitopes is further demonstrated by experience with PfEBA-175: anti-EBA-175 R217 antibodies block glycophorin A (GpA) engagement yet do not inhibit growth, whereas anti-R218 antibodies permit receptor binding yet effectively block invasion. This indicates that the functionally critical epitopes for invasion blocking may differ from those that block ligand-receptor binding alone.

4.5 Study Limitations

There are several limitations that need to be acknowledged. The WPDS screen used a small cohort (n=7), and paired pre- and post-severe malaria plasma samples may not capture the full spectrum of severe malaria-specific antibody responses. The 20% growth-inhibitory rate in

mice (out of 45 BALB/c mice) might be reflected as an epitope-dependent functional activity or a stochastic outcome of a small initial sample size. Therefore, larger immunization cohorts in multiple mouse strains are needed to establish reproducibility. The GIA was only performed using the laboratory-adapted 3D7 strain, thereby functional validation against heterologous field isolates (e.g., Dd2, additional P. falciparum field strains) is important to confirm strain-transcending inhibition for P113. Since all assays used whole immune sera, isolation of inhibitory monoclonal antibodies or testing purified IgG would strengthen the functional conclusions.

4.6 Future Directions

Building upon the findings of this thesis, several priority experiments are needed to further characterize P113 as a vaccine candidate. First, the inhibitory epitope identified by PEPperMAP (HLQGSEQSIEASESS) should be synthesized as a peptide–KLH conjugate and used to immunize mice. This immunization outcome will help testing whether focusing the immune response on the functional epitope can improve the growth-inhibitory rate beyond 20% and generate more uniform growth-inhibitory responses. Second, immunofluorescence assays (IFA) and ultrastructural expansion microscopy (U-ExM) should be performed to confirm the endogenous localization of P113 on the merozoite surface and its spatial association with PfRh5 and MSP-9. This would help strengthen the mechanistic rationale for P113 as an invasion-blocking target.

Third, one-cycle invasion assays should be conducted to determine whether anti-P113 antibodies specifically block merozoite invasion of erythrocytes, consistent with P113's proposed

role as the membrane anchor for the PfRh5:CyRPA:Ripr invasion complex. Fourth, affinity purification of IgG from inhibitory sera using Protein G columns would formally confirm that the growth-inhibitory activity is antibody-mediated rather than due to other serum factors. Moreover, the GIA should be repeated against heterologous *P. falciparum* strains (e.g., Dd2, MRA) to confirm strain-transcending inhibition, leveraging the limited sequence variation of P113 across field isolates.

Longer-term goals include evaluating P113 in combination with other Kurtis Laboratory vaccine candidates (PfSEA-1, PfGARP, PfGBP130) as part of a multi-antigen strategy that simultaneously targets merozoite invasion (P113), parasite egress (PfSEA-1), and intraerythrocytic survival (PfGARP).[17] Additionally, mechanistic studies investigating P113 interactions with PfRh5, MSP-9, and parasitophorous vacuole membrane (PVM)-associated proteins will be essential to fully define the broader biological roles of P113 in membrane architecture, protein export, and erythrocyte invasion.

References

1. White NJ, Pukrittayakamee S, Hien TT, Faiz MA, Mokuolu OA, Dondorp AM. Malaria. Lancet. 2014;383(9918):723-735. doi:10.1016/S0140-6736(13)60024-0

2. World Health Organization. World Malaria Report 2024. Geneva: WHO; 2024.

3. Desai M, ter Kuile FO, Nosten F, McGready R, Asamoa K, Brabin B, Newman RD. Epidemiology and burden of malaria in pregnancy. Lancet Infect Dis. 2007;7(2):93-104. doi:10.1016/S1473-3099(07)70021-X

4. GBD 2023 Disease and Injury and Risk Factor Collaborators. Burden of 375 diseases and injuries, risk-attributable burden of 88 risk factors, and healthy life expectancy in 204 countries and territories, including 660 subnational locations, 1990–2023: a systematic analysis for the Global Burden of Disease Study 2023. Lancet. 2025;406:1873-1922. doi:10.1016/S0140-6736(25)01637-X

5. Gallup JL, Sachs JD. The economic burden of malaria. Am J Trop Med Hyg. 2001;64(1-2 Suppl):85-96. doi:10.4269/ajtmh.2001.64.85

6. Cowman AF, Healer J, Marapana D, Marsh K. Malaria: biology and disease. Cell. 2016;167(3):610-624. doi:10.1016/j.cell.2016.07.055

7. World Health Organization. Guidelines for malaria. Geneva: WHO; 2023.

8. Casals-Pascual C, Roberts DJ. Malaria during pregnancy. Curr Mol Med. 2006;6(2):155-168. doi:10.2174/156652406776055186

9. Bhatt S, Weiss DJ, Cameron E, et al. The effect of malaria control on Plasmodium falciparum in Africa between 2000 and 2015. Nature. 2015;526(7572):207-211. doi:10.1038/nature15535

10. Ranson H, Lissenden N. Insecticide resistance in African Anopheles mosquitoes: a worsening situation that needs urgent action to maintain malaria control. Trends Parasitol. 2016;32(3):187-196. doi:10.1016/j.pt.2015.11.010

11. Woodrow CJ, White NJ. The clinical impact of artemisinin resistance in Southeast Asia and the potential for future spread. FEMS Microbiol Rev. 2017;41(1):34-48. doi:10.1093/femsre/fuw037

12. Uwimana A, Legrand E, Stokes BH, et al. Emergence and clonal expansion of in vitro artemisinin-resistant Plasmodium falciparum kelch13 R561H mutant parasites in Rwanda. Nat Med. 2020;26(10):1602-1608. doi:10.1038/s41591-020-1005-2

13. RTS,S Clinical Trials Partnership. Efficacy and safety of RTS,S/AS01 malaria vaccine with or without a booster dose in infants and children in Africa: final results of a phase 3, individually randomised, controlled trial. Lancet. 2015;386(9988):31-45. doi:10.1016/S0140-6736(15)60721-8

14. Datoo MS, Natama HM, Somé A, et al. Efficacy and immunogenicity of R21/Matrix-M vaccine against clinical malaria after 2 years' follow-up in children in Burkina Faso: a

phase 1/2b randomised controlled trial. Lancet Infect Dis. 2022;22(12):1728-1736. doi:10.1016/S1473-3099(22)00442-X

15. Thera MA, Doumbo OK, Coulibaly D, et al. A field trial to assess a blood-stage malaria vaccine. N Engl J Med. 2011;365(11):1004-1013. doi:10.1056/NEJMoa1008115

16. Ogutu BR, Apollo OJ, McKinney D, et al. Blood stage malaria vaccine eliciting high antigen-specific antibody concentrations confers no protection to young children in Western Kenya. PLoS One. 2009;4(3):e4708. doi:10.1371/journal.pone.0004708

17. Duffy PE, Gorres JP. Malaria vaccines since 2000: progress, priorities, products. npj Vaccines. 2020;5:48. doi:10.1038/s41541-020-0196-3

18. Minassian AM, Silk SE, Barrett JR, et al. Reduced blood-stage malaria growth and immune correlates in humans following RH5 vaccination. Med. 2021;2(6):701-719.e19. doi:10.1016/j.medj.2021.03.014

19. Gupta S, Snow RW, Donnelly CA, Marsh K, Newbold C. Immunity to non-cerebral severe malaria is acquired after one or two infections. Nat Med. 1999;5(3):340-343. doi:10.1038/6560

20. Gonçalves BP, Huang CY, Morrison R, et al. Parasite burden and severity of malaria in Tanzanian children. N Engl J Med. 2014;370(19):1799-1808. doi:10.1056/NEJMoa1303944

21. Raj DK, Nixon CP, Nixon CE, et al. Antibodies to PfSEA-1 block parasite egress from RBCs and protect against malaria infection. Science. 2014;344(6186):871-877. doi:10.1126/science.1254417

22. Raj DK, Mohapatra AD, Jnawali A, et al. Anti-PfGARP kills parasites by inducing PCD and attenuates severe malaria. Nature. 2020;582(7810):104-108. doi:10.1038/s41586-020-2220-1

23. Johnson Y, Shakri AR, et al. Immunization with PfGBP130 generates antibodies that inhibit RBC invasion by P. falciparum parasites. Front Immunol. 2024;15:1350560. doi:10.3389/fimmu.2024.1350560

24. Fawaz R. Identifying the Parasite Targets Mediating Resistance to Severe Malaria [master's thesis]. Providence, RI: Brown University; 2025.

25. Galaway F, Drought LG, Fber M, et al. P113 is a merozoite surface protein that binds the N terminus of Plasmodium falciparum RH5. Nat Commun. 2017;8:14333. doi:10.1038/ncomms14333

26. Cowman AF, Tonkin CJ, Tham WH, Duraisingh MT. The molecular basis of erythrocyte invasion by malaria parasites. Cell Host Microbe. 2017;22(2):232-245. doi:10.1016/j.chom.2017.07.003

27. Crosnier C, Bustamante LY, Bartholdson SJ, et al. Basigin is a receptor essential for erythrocyte invasion by Plasmodium falciparum. Nature. 2011;480(7378):534-537. doi:10.1038/nature10606

28. Douglas AD, Williams AR, Illingworth JJ, et al. The blood-stage malaria antigen PfRH5 is susceptible to vaccine-inducible cross-strain neutralizing antibody. Nat Commun. 2011;2:601. doi:10.1038/ncomms1615

29. Wong W, Huang R, Menant S, et al. Structure of Plasmodium falciparum Rh5-CyRPA-Ripr invasion complex. Nature. 2019;565(7737):118-121. doi:10.1038/s41586-018-0779-6

30. Minassian AM, Silk SE, Barrett JR, et al. Reduced blood-stage malaria growth and immune correlates in humans following RH5 vaccination. Med. 2021;2(6):701-719.e19. doi:10.1016/j.medj.2021.03.014

31. Bullen HE, Sanders PR, et al. The Plasmodium falciparum parasitophorous vacuole protein P113 interacts with the parasite protein export machinery and maintains normal vacuole architecture. Mol Microbiol. 2022;117(5):1245-1262. doi: 10.1111/mmi.14904.

32. Sapkota A. Malaria- Definition, causative agent, cycle, pathogenesis. Microbe Notes. Published 2022. Accessed April 15, 2026. https://microbenotes.com/malaria-plasmodium/

33. Miura K, Zhou H, Diouf A, et al. Anti-apical-membrane-antigen-1 antibody is more effective than anti-42-kilodalton-merozoite-surface-protein-1 antibody in inhibiting Plasmodium falciparum growth, as determined by the in vitro growth inhibition assay. Clin Vaccine Immunol. 2009;16(7):963-968. doi:10.1128/CVI.00042-09

34. Chen L, Lopaticki S, Riglar DT, et al. An EGF-like protein forms a complex with PfRh5 and is required for invasion of human erythrocytes by Plasmodium falciparum. PLoS Pathog. 2011;7(9):e1002199. doi:10.1371/journal.ppat.1002199

35. Reineke U, Volkmer-Engert R, Schneider-Mergener J. Applications of peptide arrays prepared by the SPOT-technology. Curr Opin Biotechnol. 2001;12(1):59-64. doi:10.1016/S0958-1669(00)00178-6

36. Harris JR, Markl J. Keyhole limpet hemocyanin (KLH): a biomedical review. Micron. 1999;30(6):597-623. doi:10.1016/S0968-4328(99)00036-0

37. Roser M, Ritchie H. Malaria. Our World in Data. Published 2024. Accessed April 17, 2026. https://ourworldindata.org/malaria. Data source: WHO Global Health Observatory via World Bank (2026). Licensed under CC BY 4.0.

38. Novagen. T7Select System Manual. EMD Millipore; 2011.

39. Aurrecoechea C, Brestelli J, Brunk BP, et al. PlasmoDB: a functional genomic database for malaria parasites. Nucleic Acids Res. 2009;37(Database issue):D539-D543. doi:10.1093/nar/gkn814

40. Altschul SF, Gish W, Miller W, Myers EW, Lipman DJ. Basic local alignment search tool. J Mol Biol. 1990;215(3):403-410. doi:10.1016/S0022-2836(05)80360-2

41. Trager W, Jensen JB. Human malaria parasites in continuous culture. Science. 1976;193(4254):673-675. doi:10.1126/science.781840

42. Chan M. Characterization of the Novel Antimalarial 2741-19: Barrier to resistance and Stage-Specific Activity [master's thesis]. Providence, RI: Brown University; 2026.

43. Petersen TN, Brunak S, von Heijne G, Nielsen H. SignalP 4.0: discriminating signal peptides from transmembrane regions. Nat Methods. 2011;8(10):785-786. doi:10.1038/nmeth.1701

44. Arumugam TU, Takeo S, Yamasaki T, et al. Discovery of GAMA, a Plasmodium falciparum merozoite micronemal protein, as a novel blood-stage vaccine candidate antigen. Infect Immun. 2011;79(11):4523-4532. doi:10.1128/IAI.05412-11

45. Campeotto I, Galaway F, Mehmood S, Barfod LK, Quinkert D, Kotraiah V, et al. The Structure of the Cysteine-Rich Domain of Plasmodium falciparum P113 Identifies the Location of the RH5 Binding Site. mBio. 2020;11. doi:10.1128/mBio.01566-20

46. Malaria Genomic Epidemiology Network. Reappraisal of known malaria resistance loci in a large multicenter study. Nat Genet. 2014;46(11):1197-204. doi: 10.1038/ng.3107.

Supplementary Figures

Supplementary Figure S1. PEPperMAP linear epitope mapping of mouse sera 2 and 3 against *P. falciparum* 3D7 surface protein P113. *(Top)* Mouse Serum 2 (inhibitory, 1:500 dilution): a strong polyclonal antibody response was observed with prominent peaks at multiple regions across the P113 sequence. *(Bottom)* Mouse Serum 3 (non-inhibitory, 1:500 dilution): the overall binding profile was highly similar to Mouse Serum 2, with most prominent responses shared across both serum.

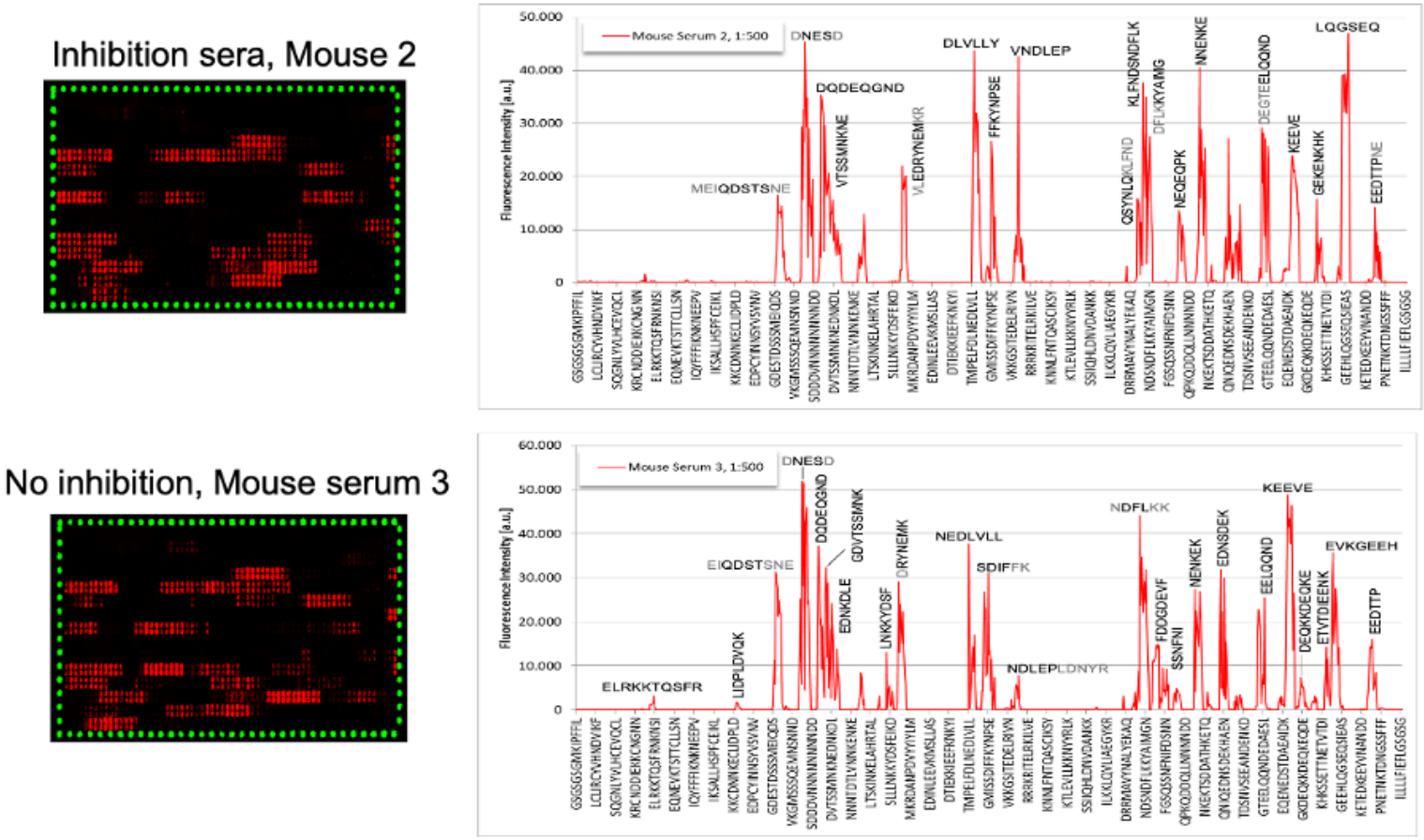

Supplementary Figure S2. PEPperMAP linear epitope profiling of mouse sera 2 and 3. Fluorescence intensity signals across overlapping peptides spanning the P113 sequence are shown for Mouse Serum 2 (inhibitory; 1:500 dilution) and Mouse Serum 3 (non-inhibitory; 1:500 dilution). Subtle differences in specific regions (arrowhead) may underlie differences in functional activity.

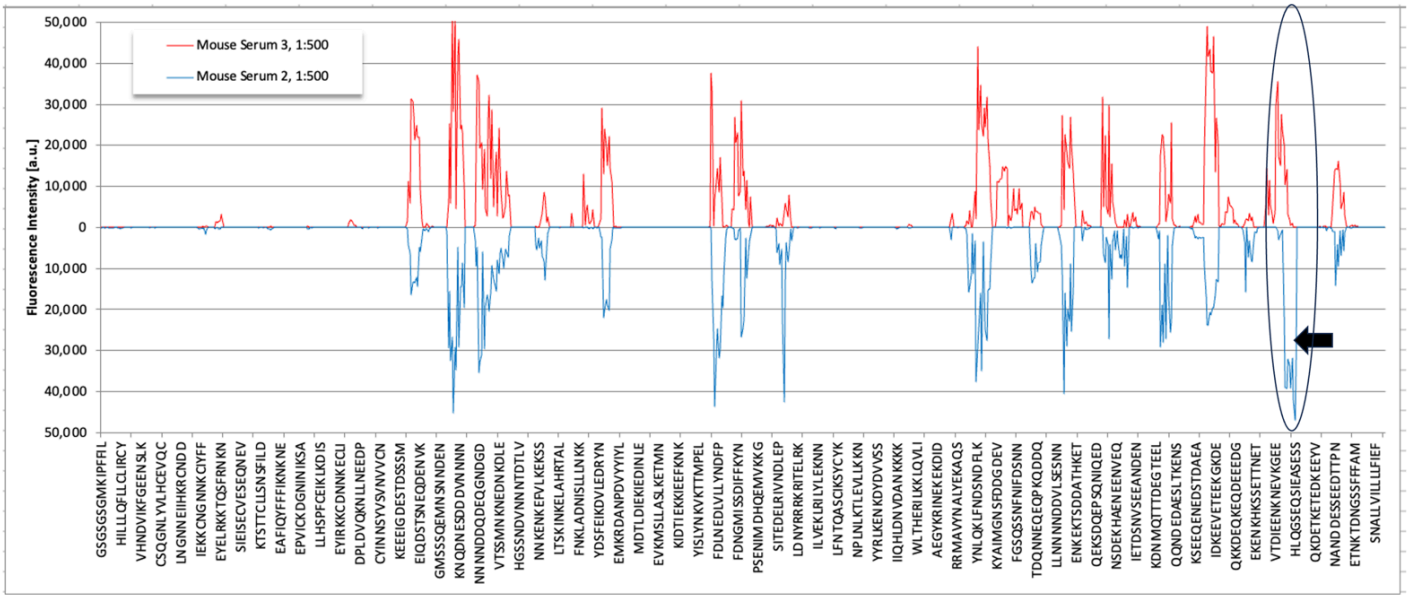

Supplementary Figure S3. Identification and validation of P113 with Mass Spec. *(Top)* Proteomic analysis of enriched phage clones identified nine *Plasmodium falciparum* 3D7 proteins. Surface protein P113 showing the highest spectral counts across independent samples (67847 and 67848). *(Middle & Bottom)* Peptide mapping of P113 from two independent samples (P113#1 and P113#2) demonstrates extensive sequence coverage (88% and 71%, respectively), with highlighted regions representing identified peptides.

Supplementary Tables

Supplementary Table 2. Parasite proteins identified by Whole Proteome Differential Screening (WPDS). Inserts from 188 plaques recovered after differential biopanning were PCR-amplified, sequenced, and identified by Megablast alignment to the P. falciparum 3D7 genome. BP3 (%) and BP4 (%) indicate the percentage of clones encoding each protein after three and four rounds of positive selection, respectively; '/' indicates the protein was not detected in that round.

Gene Name	Gene ID	BP3 (%)	BP4 (%)	MW	SignalP	TMHMM	Length
Glutamic acid-rich protein GARP	PF3D7_0113000	2.27	34.48	79795	yes	yes	673
Merozoite surface protein 4	PF3D7_0207000	/	1.38	30549	no	yes	272
Exportin-1, putative	PF3D7_0302900	21.59	2.07	147938	no	no	1254
Plasmodium exported protein	PF3D7_0402400	1.14	/	31019	no	yes	254
NYN domain-containing protein	PF3D7_0406500	/	0.69	383846	no	no	3211
Karyopherin beta	PF3D7_0524000	/	0.69	127353	no	no	1123
Conserved Plasmodium protein	PF3D7_0621000	/	0.69	100705	no	no	844
HECT-domain (ubiquitin-transferase)	PF3D7_0628100	/	0.69	1206017	no	yes	10287
Rhoptry-associated membrane antigen	PF3D7_0707300	/	2.76	1206017	no	yes	10287
Vacuolar protein sorting-assoc. protein 9	PF3D7_0815800	/	1.38	214692	no	no	1833
HECT-like E3 ubiquitin ligase	PF3D7_0826100	1.14	/	1005144	no	yes	859
Heat shock protein 70	PF3D7_0917900	2.27	2.07	72388	yes	no	652
Ring-exported protein 1	PF3D7_0935900	/	0.69	83041	no	yes	713
Ring-exported protein 2	PF3D7_0936000	5.68	/	10771	no	yes	94
PRE-binding protein	PF3D7_1011800	/	0.69	131626	no	no	1139
Conserved Plasmodium protein	PF3D7_1021200	/	3.45	82849	no	no	689
Translocon component PTEX88	PF3D7_1105600	/	0.69	90787	yes	no	777
Exported protein 1	PF3D7_1121600	/	0.69	17296	yes	yes	162

Conserved Plasmodium protein	PF3D7_1221300	1.14	/	84218	no	no	711
Conserved Plasmodium protein	PF3D7_1228700	2.27	/	136557	yes	yes	1135
Coronin	PF3D7_1251200	3.41	2.76	69015	no	no	602
Plasmodium exported protein	PF3D7_1252500	1.14	/	47312	no	yes	394
M1-family alanyl aminopeptidase	PF3D7_1311800	/	0.69	126062	no	yes	1085
Conserved protein, unknown function	PF3D7_1329500	/	0.69	218438	no	no	1844
Conserved Plasmodium protein	PF3D7_1329600	/	0.69	35019	no	no	301
Plasmepsin III	PF3D7_1408100	/	2.07	51693	no	yes	451
Surface protein P113	PF3D7_1420700	2.27	/	112574	yes	yes	969
Sortilin	PF3D7_1451800	10.23	/	102270	no	yes	895

Supplementary Table 2. Pre- and post-sample collection dates for study participants. The table lists study IDs along with the corresponding dates of sample collection prior to (pre-) and following (post-) the defined clinical timepoint. Dates are presented in DD/MM/YYYY format.

Study IDs	Pre- sample Date	Post- sample Date
CA001	30/04/2018	10/08/2018
CA057	09/10/2018	19/11/2018
CA079	30/03/2018	25/06/2018
CA130	25/9/2020	30/11/2020
CA131	30/04/2018	25/06/2018
CA155	16/07/2018	15/09/2018
CA205	10/02/2020	12/04/2020